PHYSICAL REVIEW D **94,** 063004 (2016)

Constraining the production of cosmic rays by pulsars

Mikhail M. Ivanov,[1,2,3] Maxim S. Pshirkov,[4,1,5] and Grigory I. Rubtsov[1]

[1]*Institute for Nuclear Research of the Russian Academy of Sciences, 117312 Moscow, Russia*
[2]*Faculty of Physics, Moscow State University, 119991 Moscow, Russia*
[3]*FSB/IPHYS/LPPC, École Polytechnique Fédérale de Lausanne, CH-1015 Lausanne, Switzerland*
[4]*Sternberg Astronomical Institute, Lomonosov Moscow State University, 119992 Moscow, Russia*
[5]*Pushchino Radio Astronomy Observatory, 142290 Pushchino, Russia*

(Received 7 June 2016; published 13 September 2016)

One of the possible sources of hadronic cosmic rays (CRs) are newborn pulsars. If this is indeed the case, they should feature diffusive gamma-ray halos produced by interactions of CRs with interstellar gas. In this paper we try to identify extended gamma-ray emission around young pulsars, making use of the 7-year Fermi-LAT data. For this purpose we select and analyze a set of eight pulsars that are most likely to possess detectable gamma-ray halos. We find extended emission that might be interpreted as a gamma-ray halo only in the case of PSR J0007 + 7303. Its luminosity accords with the total energy of injected cosmic rays $\sim 10^{50}$ erg, although other interpretations of this source are possible. Irrespectively of the nature of this source, we put bounds on the luminosity of gamma-ray halos which suggest that pulsars' contribution to the overall energy budget of galactic CRs is subdominant in the GeV–TeV range.

DOI: 10.1103/PhysRevD.94.063004

I. INTRODUCTION

Cosmic ray (CR) experiments have allowed for the measurement of the spectrum and chemical composition of galactic CRs. The observed value of the latter requires an average cumulative power of CR sources $L_{\rm CR} \sim 10^{41}$ erg/s [1] at energies $E_{CR} > 0.1$ GeV.

The bulk of galactic cosmic rays is widely believed to originate from supernova remnants (SNRs); see the recent reviews [2,3]. This hypothesis is supported by a number of convincing, independent, and yet circumstantial indications. The most remarkable are recent observations of the SNRs W44 and IC433 [4–6], which allowed for confident conclusions on the hadronic nature of their gamma-ray emission. Nevertheless, there are still puzzles to be resolved, e.g., a mismatch between the predicted and observed slopes of the gamma-ray spectrum. It is also not clear whether SNRs indeed accelerate CRs up to the "knee" energies $\sim 10^6$ GeV. Besides, several breaks observed in the Galactic CR spectrum [7,8] hint at the existence of multiple components in the interstellar CR flux. This motivates a search for some complementary scenarios of CR production. CRs can be produced by mechanisms operating at large scales, such as acceleration in superbubbles [9,10] or Galactic-wind shocks [11]. This scenario is supported by the chemical composition of the low-energy cosmic ray flux [12] and by the extended gamma-ray emission observed in the Cygnus superbubble [9].

Alternatively, pulsars and their pulsar wind nebulae (PWNe) could be viable sources of CRs [13–16]. Indeed, the rotation energy of neutron stars at birth is sufficient to produce the required CR power [17,18]. It is well established that the rotation energy of young pulsars is spent extremely efficiently on the production and acceleration of leptons [19–21]. Furthermore, the most successful theoretical models of particle acceleration at pulsar winds [22,23] predict that ions should typically carry energy larger than that of electrons and positrons. However, the emission associated with high-energy leptons may introduce a serious obstacle to testing the production of CRs by pulsars: the hadron component of the gamma-ray flux could be deeply hidden in the overwhelming emission of leptonic origin.

Fortunately, there is a potential way out of this predicament. When CRs escape their sources they should interact with interstellar gas and produce observable gamma-ray emission. According to an estimate given below a typical size of an extended halo around a young pulsar should be ~ 100 pc. Unlike ions, leptons undergo severe energy losses due to synchrotron emission and inverse Compton scattering. Thus, one may expect that at distances comparable to the halo size the energy density of leptons becomes suppressed [24], and gamma-ray emission is dominated by the hadronic component.

Several candidates for the extended gamma-ray halos around young pulsars were found in Ref. [18], which may be considered as evidence in favor of CR production by pulsars. Moreover, the results obtained in Ref. [18] led to the conclusion that gamma-ray halos should exist around nearly all young pulsars with a spin-down age $T_{\rm SD} \lesssim 30$ kyr. The observations of the very high-energy neutrinos reported by IceCube [25] can also be consistently interpreted within this scenario [26,27]. All of these pieces of evidence and their relevance for unveiling the puzzles of CRs suggest that the hypothesis of CR production by pulsars requires further investigation, which we perform in this paper.

This paper is organized as follows. In Sec. II we discuss theoretical aspects of CR production by pulsars and properties of hypothetical gamma-ray halos around them. Section III is devoted to the selection of pulsars for further tests. In Sec. IV we discuss the analysis of the Fermi-LAT data. In Sec. V we discuss the dependence of the statistical significance on halo fluxes retrieved from simulations. This will allow us to constrain the halo luminosity. Section VI is devoted to the analysis of the selected pulsars with the Fermi-LAT data. The results are interpreted in Sec. VII. We draw conclusions in Sec. VIII. In Appendix A we describe properties of the pulsars from Ref. [18], whereas Appendix B contains the details of the simulations. In Appendix C we verify that the sources found in Ref. [18] are not the result of statistical fluctuations. Finally, in Appendix D we show best fits for the sources from our analysis and compare them to the values from the 3FGL catalogue.

II. THEORETICAL PRELIMINARIES

In order to reproduce the observed density of CRs at Earth ~ 1 eV/cm^3 [7], one requires the following total time-averaged luminosity of CR sources [1]:

$$L_{\rm CR}^{\rm tot} \simeq 8 \times 10^{40} \frac{\rm erg}{\rm s}. \quad (1)$$

Notice that this is the total power of hadrons and nuclei with kinetic energies $E_{\rm CR} \gtrsim 0.1$ GeV.

The most plausible sources of this power are supernovae explosions, which release $\sim 10^{51}$ erg with the rate $(1/30 - 1/130)$ yr^{-1} [28]. Indeed, a rough estimate implies that some $\sim 10\%$ of this energy would totally account for the bulk of galactic cosmic rays,

$$L_{\rm SN}^{\rm CR} \sim \mathcal{E}_{\rm CR}^{\rm tot} \mathcal{R}_{\rm SN} \simeq 10^{41} \frac{\rm erg}{\rm s} \left[\frac{\mathcal{E}_{\rm CR}^{\rm tot}}{2 \times 10^{50}\ {\rm erg}}\right] \left[\frac{\mathcal{R}_{\rm SN}}{1/50\ {\rm yr}^{-1}}\right], \quad (2)$$

where $\mathcal{E}_{\rm CR}^{\rm tot}$ is the total energy output per supernova in the form of CRs.

As another option, the required energy input can be provided by fast-spinning newborn pulsars [17,18], which possess a sufficient amount of rotational energy,

$$E_{\rm rot} = \frac{I_{\rm NS}\Omega^2}{2} \simeq 2 \times 10^{50}\ {\rm erg} \left[\frac{I_{\rm NS}}{10^{45} {\rm g\ cm}^2}\right] \left[\frac{10\ {\rm ms}}{P_{\rm ini}}\right]^2. \quad (3)$$

In fact, theoretical models predict that initial periods of neutron stars at birth can be even shorter than 1 ms in the absence of strong magnetic coupling between a stellar core and outer layers [29].

The pulsar birthrate should typically be smaller than the core-collapsed supernova rate; thus, if young pulsars are the only source of CRs they should inject more CRs than is expected from supernovae. Unfortunately, current measurements of the pulsar birthrate are less certain than those of the supernova rate [30,31]. Hence, we stick to the latter in this paper. The uncertainly in the supernova rate induces a significant scatter over the required energy,

$$\mathcal{E}_{\rm CR}^{\rm tot} \simeq (1 - 5) \times 10^{50}\ {\rm erg}. \quad (4)$$

When released, the cosmic rays generated by a pulsar diffuse away through the Galactic magnetic field and fill a spherical volume whose radius can be estimated as

$$r_{\rm CR} \simeq 2\sqrt{D T_{\rm SD}}, \quad (5)$$

where D is the energy-dependent diffusion coefficient and $T_{\rm SD}$ is the pulsar's spin-down age, which can be taken as an estimate for the typical time passed since the CRs' emission. The diffusion coefficient D is given by [1,32]

$$D = D_{28} \times 10^{28} \left[\frac{E_{\rm CR}}{3\ {\rm GeV}}\right]^{\delta} {\rm cm}^2/{\rm s},$$
$$\delta = 0.4 \pm 0.1, \quad (6)$$

where the prefactor $D_{28} \sim 1$ and we assumed that the rigidity of CRs is the same as that of protons. Notice that the uncertainty of the prefactor D_{28} is up to a factor of 3. The size of the CR halo around a pulsar (5) is given by[1]

$$r_{\rm CR} \simeq 120 \times D_{28}^{1/2} \left[\frac{T_{\rm SD}}{10\ {\rm kyr}}\right]^{1/2} \left[\frac{E_{\rm CR}}{1\ {\rm TeV}}\right]^{0.2} {\rm pc}. \quad (7)$$

As CRs interact with the interstellar medium, the CR halo should have a gamma-ray counterpart. In what follows we will assume a typical energy yield in gamma rays $\kappa \approx 0.2$. This value for the yield is shown to agree quite well with precise numerical calculations [33,34].

One finds that the characteristic angular size of the gamma-ray halo scales with $T_{\rm SD}$, the photon energy $E_\gamma = \kappa E_{\rm CR}$, and the distance to the source r_s as

$$R_{\rm halo} = \frac{r_{\rm CR}}{r_s} \simeq 1.4^\circ D_{28}^{1/2} \left[\frac{5\ {\rm kpc}}{r_s}\right] \left[\frac{T_{\rm SD}}{10\ {\rm kyr}}\right]^{1/2} \left[\frac{E_\gamma}{200\ {\rm GeV}}\right]^{0.2}. \quad (8)$$

In what follows we will use uppercase letters R to denote angular distances and lowercase letters r to denote physical distances.

[1]In Ref. [18] the same estimate yielded a slightly smaller distance $r_s = 80$ pc. However, this numerical inaccuracy does not alter any results.

The protons and nuclei produce gamma rays in inelastic collisions with interstellar nucleons mostly due to the production and subsequent decay of π^0 mesons. The cross section for the inelastic pp scattering has a logarithmic dependence on $E_{\rm CR}$ and declines abruptly at energies $E_{\rm CR} \lesssim 2$ GeV [35]. Thus, the resulting gamma-ray spectrum of a halo should be dominated by photons with energies $E_\gamma \gtrsim 0.5$ GeV. Nevertheless, we will see in what follows that the gamma-ray halos can be unambiguously detected only at energies $E_\gamma \gtrsim 1$ GeV. Hence, the relevant energy range of CRs contributing to this emission is $E_{\rm CR} \gtrsim 5$ GeV.

The luminosity of this halo can be estimated using a typical interaction time of CRs in the interstellar medium (ISM),

$$t_{\rm int} = \frac{1}{c\sigma_{pp} n_{\rm ISM}} \simeq 3\times 10^7 \left[\frac{1\ {\rm cm}^{-3}}{n_{\rm ISM}}\right]\ {\rm yr}, \tag{9}$$

where we have taken $\sigma_{pp} = 3\times 10^{-26}$ cm^2 as an average cross section for the inelastic pp scattering for protons with $E_{\rm CR} > 5$ GeV [35], and the *average* interstellar matter density in the Galactic disc is $n_{\rm ISM} \sim 1$ cm^{-3} [36]. Making use of Eq. (9), one obtains the following halo luminosity:

$$L_\gamma^{E_\gamma \gtrsim 1\ {\rm GeV}} \sim \kappa \frac{\mathcal{E}_{\rm CR}^{\rm halo}}{t_{\rm int}} \simeq 4\times 10^{34} \left[\frac{\kappa}{0.2}\right] \left[\frac{\mathcal{E}_{\rm CR}^{\rm halo}}{2\times 10^{50}\ {\rm erg}}\right] \left[\frac{n_{\rm ISM}}{1\ {\rm cm}^{-3}}\right] \frac{\rm erg}{\rm s}, \tag{10}$$

where $\mathcal{E}_{\rm CR}^{\rm halo}$ is the total energy of cosmic rays with $E_{\rm CR} \gtrsim 5$ GeV injected by a pulsar.

It should be pointed out that accurate numerical calculations [33,34,37] imply that for realistic CR spectra the spectrum of produced gamma rays has a maximum at $E_\gamma \simeq 1$ GeV and drops sharply at lower energies. Thus, one can think of $\mathcal{E}_{\rm CR}^{\rm halo}$ as the total energy of *all* CRs produced by a pulsar.

The candidates for the gamma-ray halos around pulsars were found in Ref. [18] using the 3-year Fermi-LAT data above 100 GeV. These candidates will be referred to as N-S sources in what follows. The N-S sources are listed in Table II of Ref. [18] and have the following typical fluxes:

$$F^{E_\gamma > 100\ {\rm GeV}} \simeq 5\times 10^{-11} \left[\frac{5\ {\rm kpc}}{r_s}\right]^2 \frac{\rm erg}{{\rm cm}^2\cdot{\rm s}}. \tag{11}$$

Assuming a power-law spectrum of photons with $\Gamma = 2$, one obtains[2] the following flux above 1 GeV:

$$F^{E_\gamma \geq 1\ {\rm GeV}} \simeq 2\times 10^{-10} \left[\frac{5\ {\rm kpc}}{r_s}\right]^2 \frac{\rm erg}{{\rm cm}^2\cdot{\rm s}}, \tag{12}$$

yielding the luminosity

$$L_\gamma^{E_\gamma \geq 1\ {\rm GeV}} = F^{E_\gamma \geq 1\ {\rm GeV}} 4\pi r_s^2 \simeq 6\times 10^{35} \frac{\rm erg}{\rm s}, \tag{13}$$

which is 20 times larger than our estimate (10). This mismatch can explained by the fact that almost all of the N-S sources are situated in the Norma arm, a peculiar star-forming region with a high-density interstellar medium. This point will be discussed in more detail in Sec. VII.

There can be several difficulties with the identification of gamma-ray halos in data, e.g., an overlap with other gamma-ray sources and background uncertainties. Postponing for a moment statistical and instrumental ambiguities (to be discussed later), we focus now on some theoretical issues which can have an impact on observations.

Pulsars are often located in the vicinity of SNR shells, many of which are associated with extended gamma-ray sources. Thus, one might worry about the disentanglement between SNRs and gamma-ray halos. The SNRs, however, have much smaller angular extension compared to CR halos. Indeed, in the adiabatic Sedov-Taylor phase [38,39] the SNR radius can be estimated as

$$r_{\rm SNR} \approx \left(\frac{25\mathcal{E}_{\rm SN}}{4\pi\rho_0}\right)^{0.2} t^{0.4}, \tag{14}$$

where $\mathcal{E}_{\rm SN}$ is the energy of the supernova explosion and ρ_0 is the preexplosion density of the interstellar medium. This implies that the observed angular size of the supernova remnant scales with time and distance as

$$R_{\rm SNR} = \frac{r_{\rm SNR}}{r_s} \simeq 0.1^\circ \left[\frac{5\ {\rm kpc}}{r_s}\right] \left[\frac{t}{10\,{\rm kyr}}\right]^{0.4} \times \left[\frac{\mathcal{E}_{\rm SN}}{10^{51}\ {\rm erg}}\right]^{0.2} \left[\frac{1\ {\rm cm}^{-3}}{n_{\rm ISM}}\right]^{0.2}, \tag{15}$$

where we assumed that the ISM is composed of protons and used the relation $\rho_0 = m_p n_{\rm ISM}$. The dependence on the supernova energy output and the density of the interstellar medium is quite mild, and the angular size of SNRs is defined, in essence, by distance and age. From Eqs. (15) and (8) it can be seen that the SNR radius is smaller than the radius of a gamma-ray halo at energies $E_\gamma \gtrsim 1$ GeV. This suggests that our analysis should be performed in this energy range in order to avoid a possible overlap between the halos and SNRs.[3]

[2]We adopt $\Gamma = 2$ here in order to obtain a conservative estimate for the total luminosity.

[3]There can also be a PWN, but its typical extension ~10 pc is very small compared to that of SNRs or the gamma-ray halos we discuss. The results of this paper will be valid for systems which contain both pulsars and PWNe.

The presence of a SNR or PWN around a pulsar may complicate the escape of GeV particles; see Refs. [2,40]. However, as pointed out in these references, there are several reasons to expect that particle confinement does not necessarily take place even in the case of perfectly continuous shells, e.g., because of cross-field diffusion.

In principle, one can expect that a gamma-ray halo and the host pulsar can be offset due to the pulsar kick. This offset is, however, quite small for young pulsars with $T_{\rm SD} \lesssim 10^4$ yr and cannot exceed (see Ref. [41] for typical kick velocities)

$$\Delta R \simeq 0.1^\circ \left[\frac{5\ \mathrm{kpc}}{r_s}\right]\left[\frac{v}{10^3\ \mathrm{km/s}}\right]\left[\frac{T_{\rm SD}}{10\,\mathrm{kyr}}\right]. \quad (16)$$

This offset is small compared to the angular size of the gamma-ray halo and we will neglect it in what follows.

III. PULSAR SAMPLE

In Ref. [18] Neronov and Semikoz identified 18 degree-scale extended sources (to be referred to as *N-S sources* after the authors of Ref. [18] in what follows), most of which spatially coincide with young pulsars with $T_{\rm SD} \lesssim 30$ kyr. The most straightforward approach would be to directly analyze these sources with an extended set of Fermi-LAT data. However, there are several issues which complicate the direct analysis. All but one (17 out of 18) of the *N-S* candidates are located very close to the Galactic plane, $|b| < 1^\circ$. This increases the possibility of background contamination and projection effects, which may result in a false discovery of a halo.

Most *N-S* candidates either adjoin or spatially coincide with several extended and point-like very high-energy (VHE) sources, which makes it practically impossible to disentangle extended halos from the collective emission of these sources. It should be noted that these sources may in fact be inhomogeneities of halos themselves, and further investigation of this possibility is needed. Some *N-S* candidates are so close to one another (e.g., sources No 4,5, and 6 from Table II of Ref. [18]) that they form a single "cluster" that covers multiple VHE sources. A few *N-S* sources can be associated with several pulsars, which further obscures their study.

In order to overcome these difficulties we follow an alternative method, which is to seek gamma-ray halos in an independent "cleaner" set of young pulsars. For this purpose we singled out eight sufficiently isolated young nearby pulsars located quite away from the Galactic plane. In order to select these pulsars we used the ATNF catalogue [42,43] and imposed several restrictions on the pulsars' properties and location. We put the following cuts on spin-down ages and distances:

$$T_{\rm SD} < 30\ \mathrm{kyr}, \qquad r_s < 5\ \mathrm{kpc}, \quad (17)$$

which select sufficiently nearby pulsars whose hypothetical halos should have sizable fluxes and angular extensions, and thus should be better distinguishable in the data.

In order to decrease the influence of the Galactic plane and the Galactic center, we chose the following range of Galactic coordinates:

$$15^\circ < l < 345^\circ, \qquad |b| > 1^\circ. \quad (18)$$

We obtained the set of pulsars listed in Table I. Note that we excluded the Vela pulsar which is very close ($r_s = 0.28$ kpc) and relatively old ($T_{\rm SD} = 11.3$ kyr). The gamma-ray halo around this pulsar should have an angular size so large [$R_{\rm halo}(1\ \mathrm{GeV}) \sim 10^\circ$; see Eq. (8)] that current diffuse models do not allow for its study [44].

One can check that the distance from the Galactic disc is smaller than 200 pc for all of the pulsars except PSR J0007 + 7303. Thus, these pulsars are still situated in the dense part of the neutral hydrogen (HI) disc where there should be enough target material [45]. As for PSR J0007 + 7303, a recent analysis suggests the average ISM density $n_{\rm ISM} \sim 0.1\ \mathrm{cm}^{-3}$ [46], which implies that the halo around this pulsar could still have a sizable flux.

Before moving on, we check that our sample of pulsars belongs to a population similar to that of the pulsars listed in Table II of Ref. [18] (they will be referred to as *N-S pulsars* in what follows). We have already imposed an upper bound on pulsar ages [Eq. (17)] which was suggested in Ref. [18]. In the scenario of CRs generated due to the pulsar rotational energy one might be interested in initial rotation periods and energy loss rates. These initial properties can be obtained only if the pulsar age is known independently from the spin-down, which is possible only in rather specific circumstances [47,48]; this is why we instead focus on current periods and energy losses.

Using the ATNF database we found these quantities for the *N-S* pulsars and the pulsars from our set (see Table I and Table III in Appendix A). In order to prove that the selected set of pulsars belongs to the same population as the *N-S* pulsars, we perform a two-sample Kolmogorov-Smirnov (KS) test over the values of P and $\dot{E}$ (for details, see Appendix A). We find very large p-values for either case, $p_{\rm KS} \sim 0.7$, which implies that the *N-S* sample and our

TABLE I. Pulsars selected for likelihood analysis.

	PSRJ	l	b	r_s, kpc	$T_{\rm SD}$, kyr	$\dot{E}$, erg/s	P, s
1	J0007+7303	119.66	10.46	1.40	13.9	4.5×10^{35}	0.32
2	J0501+4516	161.55	1.95	2.20	15.7	1.2×10^{33}	5.8
3	J1709−4429	343.10	−2.69	2.60	17.5	3.4×10^{36}	0.10
4	J2229+6114	106.65	2.95	3.00	10.5	2.2×10^{36}	0.052
5	J0205+6449	130.72	3.08	3.20	5.37	2.7×10^{37}	0.065
6	J1357−6429	309.92	−2.51	4.09	7.31	3.1×10^{36}	0.17
7	J0534+2200	184.56	−5.78	2.00	1.26	4.5×10^{38}	0.033
8	J1513−5908	320.32	−1.16	4.40	1.56	1.7×10^{37}	0.15

sample indeed have statistically indistinguishable distributions over $\dot{E}$ and P.

The sizes of the halos around selected pulsars are computed at different energies using Eq. (8) and listed in Table II. Comparing Tables I and II, one may notice that the sample of pulsars we selected is not totally homogeneous with respect to pulsar ages, spin-down luminosities, and the sizes of halos. There is a subset of very young pulsars with $T_{\rm SD} < 10$ kyr and large energy losses,

$$10^{36}\ \text{erg/s} \lesssim \dot{E} \lesssim 10^{38}\ \text{erg/s},$$

which includes PSR J0205 + 6449, PSR J1357 − 6429, Crab (PSR J0534 + 2200), and PSR J1513 − 5908. The halos around these pulsars have quite small angular extension (see Table II), which is why we will dub them *pulsars with compact halos* in what follows. For energies $E_\gamma \simeq 1$–10 GeV the sizes of their halos appear to be roughly equal to the LAT point spread function (PSF) in this range,

$$R_{\rm halo}(1\text{–}10\ \text{GeV}) \sim R_{\rm PSF}(1\text{–}10\ \text{GeV}) \sim 0.5^\circ. \quad (19)$$

A broad PSF worsens the localization capability and implies that halo photons from the energy bin 1–10 GeV have less statistical significance. Thus, the data in this energy range are less sensitive to compact gamma-ray halos. On the other hand, from 1 to 30 GeV the PSF falls from 0.8° down to 0.1° [49] and stays nearly constant at higher energies. On the contrary, the halo size increases according to Eq. (8), which facilitates the detection of halos by Fermi-LAT at energies $E_\gamma > 10$ GeV.

The remaining four pulsars from our set (PSR J0007 + 7303, PSR J0501 + 4516, PSR J1709 − 4429, and PSR J2229 + 6114) form a subsample of relatively old ($10\,\text{kyr} < T_{\rm SD} < 30$ kyr) pulsars with moderate energy losses,

$$10^{33}\ \text{erg/s} \lesssim \dot{E} \lesssim 10^{36}\ \text{erg/s}.$$

Looking at Table II, one can make sure that the size of the LAT PSF is smaller than the angular extension of gamma-ray halos around these pulsars above 1 GeV. This means that the halos should be better observed in the energy bin 1–10 GeV where one can expect the largest flux. We will refer to this subset of pulsars as *pulsars with large halos*.

TABLE II. Theoretical expectations for the sizes of the gamma-ray halos at different energies.

	PSRJ	$R_{\rm halo}$(1 GeV)	$R_{\rm halo}$(10 GeV)	$R_{\rm halo}$(100 GeV)
1	J0007 + 7303	2.0°	3.2°	5.0°
2	J0501 + 4516	1.4°	2.2°	3.5°
3	J1709 − 4429	1.2°	2.0°	3.1°
4	J2229 + 6114	0.8°	1.3°	2.1°
5	J0205 + 6449	0.6°	0.9°	1.4°
6	J1357 − 6429	0.5°	0.8°	1.3°
7	J0534 + 2200	0.4°	0.7°	1.1°
8	J1513 − 5908	0.2°	0.4°	0.6°

IV. DATA ANALYSIS

In our analysis we use the Fermi-LAT data collected during 361 weeks from August 4, 2008 (MET = 239557418 s) to July 6, 2015 (MET = 457859500). We use the Fermi science tools[4] (version v10r0p5), including the Pass 8 reconstruction (P8R2_SOURCE_V6). We have selected events belonging to the "SOURCE" class in order to have a reasonable number of events of good quality. When processing the data, we strictly followed the routine described in Ref. [50], which included the zenith angle cut of 90°. Moreover, data collected while the observatory was passing across the South Atlantic Anomaly were not taken into consideration.

In order to trace the variation of the halo size with energy as predicted by Eq. (8) we split the data into three different energy bins, 100–500, 10–100, and 1–10 GeV, and analyze them separately. The selected events with energies $1\ \text{GeV} \le E_\gamma \le 500$ GeV have relatively small PSF values, $R_{\rm PSF} < 0.8^\circ$ which allows us to use smaller regions of interest (RoIs). In practice, we take a circle of radius 10° around each pulsar. The data are analyzed using the binned likelihood approach implemented in the *gtlike* utility, in which two model hypotheses are compared by their maximal likelihoods with respect to the observed photon distribution. The null hypothesis does not include new sources compared to the 3FGL catalogue [49], while the alternative hypothesis assumes a halo around a selected pulsar added into the list of sources of the null hypothesis.

The null source model for each pulsar includes all of the sources from the 3FGL catalogue taken within a 10° radius around the selected pulsar, the corresponding galactic interstellar emission model *gll_iem_v06.fits*, and the isotropic spectral template *iso_P8R2_SOURCE_V6_v06.txt*. We use the spectral models from 3FGL and keep spectral parameters free for all sources within the RoI in the likelihood optimization procedure.

Now we discuss how the sources associated with the pulsars of interest are modeled in the 3FGL catalogue and hence in our input models. The pulsar PSR J0501 + 4516 (No 2 in Table I) has a rather long period and low spin-down luminosity; it does not have any gamma-ray counterpart in 3FGL and hence is absent in our model. The pulsar No 8 (PSR J1513 − 5908) is modeled in 3FGL as a point-like source while its PWN MSH 15-52 is modeled as a separate extended source of size 0.04° × 0.11°. A complex spectrum of the Crab source (No 7 in our list) has been reconstructed in 3FGL by means of three different components [49]: the gamma-pulsar

[4] http://fermi.gsfc.nasa.gov/ssc/data/analysis/.

with an exponential cutoff, a soft power-law synchrotron emission of the Crab PWN, and a hard power-law inverse Compton emission of this PWN. The sources associated with the pulsars No 1, 3, 4, and 5 are modeled with the exponential cutoff power-law spectrum typical for pulsars. The source associated with the pulsar No 6 is modeled as a point source with a power-law spectrum, which suggests that it corresponds to a pulsar-PWN system.

For the alternative hypothesis, on top of the LAT sources discussed above we have added spatial templates centred at the pulsars' coordinates taken from the ATNF database. For the extended halos we use the simplest spatial models: uniformly bright circles of different radii (from 0 to 5 degrees with a 0.1 degree step).

We use the simplest spatial model of a uniformly bright disc to remain maximally model independent. This is obviously an oversimplification, since it is expected that halos can have more complex morphology [51–53]. However, recent studies imply that the use of the simplest templates is quite robust: it does not drastically alter the statistical significance of halo detection along with best-fit values of fluxes and spectral indices [54].

The spectrum of the gamma-ray halos was taken as a simple power law,

$$\frac{dN}{dE} = N_0 \left(\frac{E}{E_0}\right)^{-\Gamma}, \tag{20}$$

where the normalization factor N_0 and the spectral index Γ are allowed to vary during the likelihood analysis, while the energy E_0 is fixed at 1 GeV.

The evidence of the detection of extended gamma-ray emission around the pulsars is evaluated in terms of the likelihood ratio test statistic (TS):

$$TS = -2 \ln \frac{L_{\max,0}}{L_{\max,1}}, \tag{21}$$

where $L_{\max,0}$ and $L_{\max,1}$ are the maximum likelihood values obtained when fitting the observed data using the null and alternative hypothesis, respectively. Note that $\sqrt{TS}$ is approximately equivalent to the source detection significance.

V. SIMULATIONS

Before analyzing the real Fermi data, in order to estimate the sensitivity of our method to gamma-ray halos we apply our method to the simulated event sets that include the halo in the source model.

Our sample of pulsars is divided into two subsets, which have different properties and are expected to be pretty different from the observational point of view. In order to understand these differences we chose to simulate one pulsar from each subset. We chose the pulsar No 1 (PSR J0007 + 7303) to represent the pulsars with large halos and the pulsar No 8 (PSR J1513 − 5908) to represent the pulsars with compact halos. These pulsars are bracketing cases for our set. The pulsar PSR J0007 + 7303 is very close, located far away from the Galactic plane and its halo should have the biggest angular extension among other pulsars. On the contrary, the pulsar PSR J1513-5908 is the farthest away, located close to the Galactic plane, and has the smallest angular size of a hypothetical halo.

In this section we briefly report the main outcome of our simulations performed with the use of the *gtobssim* utility. The details may be found in Appendix B. The simulated events are processed using the *gtlike* utility analogous to the real data (see Sec. IV).

For either pulsar we simulate two different types of gamma-ray halos. We call them *bright* and *faint* halos. For the bright halos we assume the fluxes as reported by Ref. [18] [of order Eq. (11) in the energy bin 100–500 GeV, or, equivalently, the overall luminosities of order Eq. (13)]. Our results imply that in this case gamma-ray halos will be detectable around all of the pulsars from our set in all three energy bins at quite high statistical significance.

In the case of faint halos we follow a more phenomenological approach. For either pulsar we seek the flux which produces the signal with significance $TS \sim 100$ in at least one of the energy bins. As anticipated, the sensitivity appears to be quite different for the two subpopulations of pulsars (see Fig. 1).

By scanning over different values of fluxes we find that in the case of pulsars with large halos our method is most sensitive to their fluxes in the energy bin 1–10 GeV (see the upper panel of Fig. 1), in which the flux $F^{1\text{–}10\ \mathrm{GeV}} \simeq 5 \times 10^{-9}$ ph/cm^2 s yields a halo detection with the desired significance.

On the contrary, the compact halos appear to be more easily detectable in the energy bin 10–100 GeV because of the lack of resolution at 1–10 GeV (see the lower panel of Fig. 1). We find that the flux $F^{10\text{–}100\ \mathrm{GeV}} \simeq 6 \times 10^{-10}$ ph/cm^2 s leads to a halo detection at $TS \sim 100$, while a detection at the same significance in the energy bin 1–10 GeV requires an order of magnitude larger flux in this bin.

We study the dependence of test statistics on the halo flux. For that we vary the input flux and find the resulting values of maxima of corresponding TS curves (See Fig. 2). As a result, we obtain the following scaling:

$$\begin{aligned} TS_{1\text{–}10} &\simeq 100 \left[\frac{F^{1\text{–}10\ \mathrm{GeV}}}{4.6 \times 10^{-9}\ \mathrm{ph/cm^2\ s}}\right]^{1.54}, \\ TS_{10\text{–}100} &\simeq 100 \left[\frac{F^{10\text{–}100\ \mathrm{GeV}}}{5.7 \times 10^{-10}\ \mathrm{ph/cm^2\ s}}\right]^{1.42}, \\ TS_{100\text{–}500} &\simeq 100 \left[\frac{F^{100\text{–}500\ \mathrm{GeV}}}{2.4 \times 10^{-10}\ \mathrm{ph/cm^2\ s}}\right]^{1.33}, \end{aligned} \tag{22}$$

which holds true if the angular size of the halo is larger than the LAT PSF. The dependence of this scaling on other parameters (e.g., the halo spectral index, the galactic

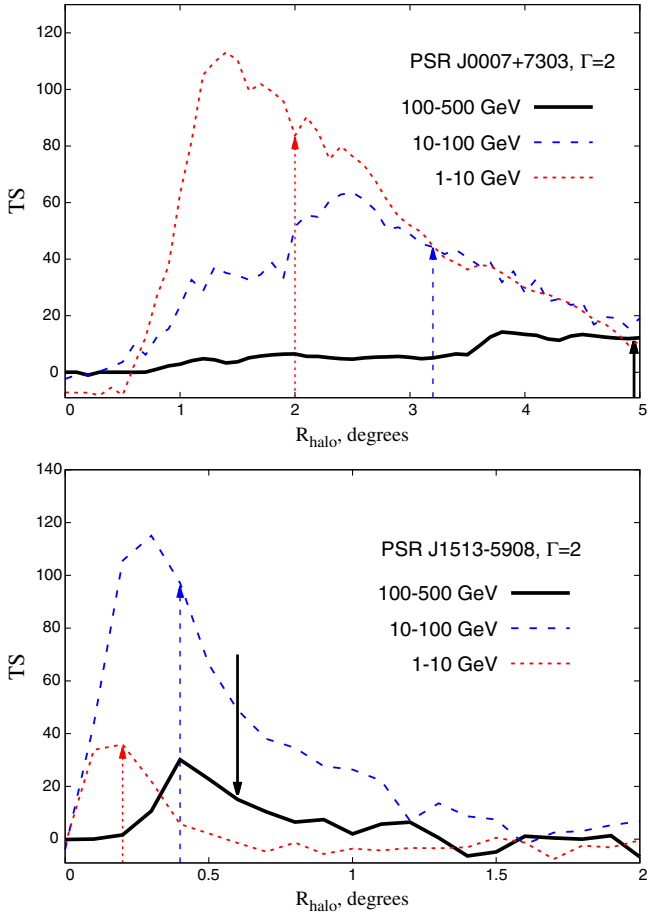

FIG. 1. $TS(R_{\rm halo})$ curves for the simulated *faint* gamma-ray halos around the pulsar PSR J0007 + 7303 (upper panel) and PSR J1513 − 5908 (lower panel); see Appendix B. The results of the analysis in different energy bands are shown as a black solid line for 100–500 GeV, a blue dashed line for 10–100 GeV, and a red dotted line for 1–10 GeV. Vertical arrows show the sizes of the halos that were used in the simulations.

latitude, etc.) is found to be quite mild and cannot exceed 20% for the range of interest $10 \lesssim TS \lesssim 100$; see Appendix B for more details.

Our analysis implies that the scaling in the energy bins 10–100 GeV and 100–500 GeV given in Eq. (22) is a generic feature valid for any halo from both subpopulations. On the contrary, the scaling in the energy bin 1–10 GeV holds only for pulsars with large halos.

VI. RESULTS

In this section we report the results of searches for the gamma-ray halos in the 7-year Fermi-LAT data. We discuss separately the outcome of our study for either subpopulation of pulsars from Table I.

A. Pulsars with large halos

As discussed in the previous section, the pulsars with large halos are the best targets for our method because it is most sensitive to halo fluxes in the energy bin 1–10 GeV where one expects the strongest signal. That is why, if CR halos exist, they are likely to be detected in this set of pulsars.

The analysis of the pulsar PSR J0007 + 7303 reveals a degree-scale excess with $TS = 89$ ($\sim 9.5\sigma$) in the energy range 1–10 GeV. This signal (see the upper panel of Fig. 3) can be compared to the simulations; see Figs. 1 and 8. Given some common features, one can interpret this excess as a gamma-ray halo produced by CRs. The small excess with $TS = 13$ at $R_{\rm halo} \approx 4.2°$ in the energy bin 10–100 GeV can also be interpreted as a counterpart of the signal seen in the bin 1–10 GeV. The data in the energy bin 1–10 GeV yield the following fit for the flux and spectral index at $R_{\rm halo} = 1.1°$:

$$F^{1\text{–}10\ \rm GeV} = (3.53 \pm 0.23) \times 10^{-9}\ \text{photons/cm}^2\,\text{s},$$
$$\Gamma = 2.798 \pm 0.081. \quad (23)$$

On the other hand, this excess may be associated with SNR CTA1 (G119.5 + 10.2) or a PWN. The extended gamma-ray emission (0.1–100 GeV) of size $0.6° \pm 0.3°$ at the position of SNR CTA1 was discovered in the energy band 0.1–100 GeV in Ref. [55]. Moreover, the extended TeV emission of size $0.3° \times 0.24°$ in the vicinity of PSR J0007 + 7303 was reported by VERITAS [56]. This emission was suggested to be associated with a PWN, which is supported by observations in other energy bands [46,57,58]. Note, however, that the extension of this emission is much smaller compared to the size of excess that we found. Thus, the presence of a compact PWN does not exclude the interpretation of the degree-scale gamma-ray emission as a CR halo.

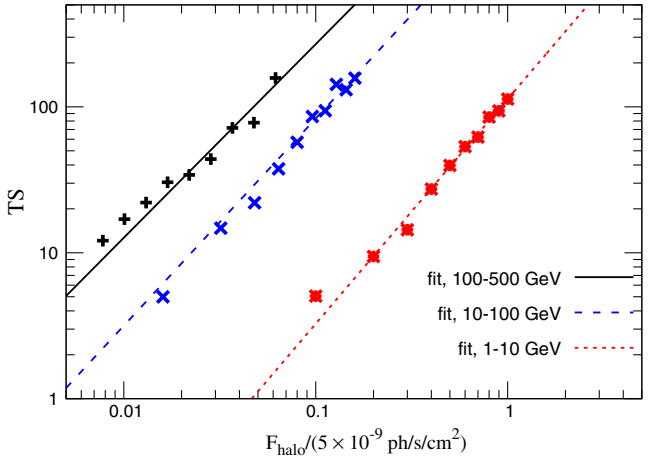

FIG. 2. The $TS(F_{\rm halo})$ dependence retrieved from simulations. Data points are taken from maxima of measured TS curves, and the lines represent best fits given in Eq. (22). The events used to produce this plot are generated for a halo around PSR J0007 + 7303 with $\Gamma = 2$; see Appendix B 1 for more details.

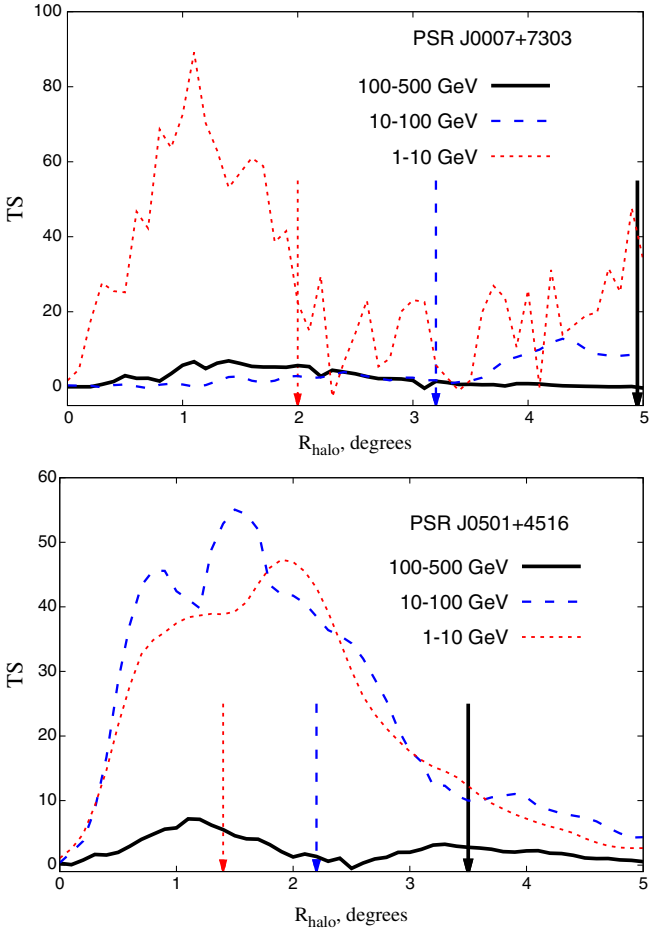

FIG. 3. $TS(R_{\rm halo})$ curves for PSR J0007 + 7303 (upper panel) and PSR J0501 + 4516 (lower panel). The results of the analysis in different energy bands are shown as a black solid line for 100–500 GeV, a blue dashed line for 10–100 GeV, and a red dotted line for 1–10 GeV. Vertical arrows show the sizes of the halos that are expected from the estimate (8).

Let us estimate the total luminosity of this halo. Using the best fit (23) and assuming that the halo spectrum has the same power-law index at energies above 10 GeV, one can find the total flux (notice that we switched to the erg/cm^2 s units),

$$F^{E_\gamma \geq 1\ \mathrm{GeV}} \simeq 1.3 \times 10^{-11}\ \mathrm{erg/cm^2\,s}, \tag{24}$$

which yields the luminosity

$$L_\gamma^{E_\gamma \geq 1\ \mathrm{GeV}} \simeq 3.0 \times 10^{33}\ \mathrm{erg/s}. \tag{25}$$

Since a part of the signal we are looking for may be already absorbed in 3FGL sources, we also keep their spectral parameters free during our analysis. Their values for PSR J0007 + 7303 can be found in Appendix D.

When analyzing the region near the pulsar PSR J0501 + 4516 we find an excess in the energy bands 10–100 GeV and 1–10 GeV at statistical significance $TS \simeq 45$ and $TS \simeq 55$, respectively, and the corresponding halo size is roughly 1.5° (see the lower panel of Fig. 3).

In fact, the region of interest has been studied in detail in Ref. [59]. This study has revealed the presence of a significantly extended ($R = 1.2° \pm 0.3°$) gamma-ray source at the position of SNR HB9 [SNR G160.4 + 02.8, $(l, b) = (160.4°, 2.75°)$]. With the new Fermi-LAT data we rediscovered this source, but its interpretation as a CR halo does not seem to be plausible. The angular size of a CR halo is expected to increase with energy, while the size of the observed emission stays nearly similar in both energy bins, which suggests that this emission may be attributable to a SNR. Because of this source, it is practically impossible to extract the signal from a hypothetical gamma-ray halo. One can, however, place a trivial bound from the fact that the halo flux in the energy bin 1–10 GeV is smaller than the total observed flux. Using the best fit for the extended emission at $R_{\rm halo} = 1.9°$, we get

$$F^{1\text{–}10\ \mathrm{GeV}} < F_{\rm tot}^{1\text{–}10\ \mathrm{GeV}} = (2.82 \pm 0.42) \times 10^{-9}\ \mathrm{ph/cm^2\,s}. \tag{26}$$

Assuming the spectral index of a halo above 10 GeV $\Gamma = 2.4$, this yields the following bounds on the overall flux and luminosity of the halo above 1 GeV:

$$F^{E_\gamma \geq 1\ \mathrm{GeV}} < 1.7 \times 10^{-11}\ \mathrm{erg/cm^2\,s},$$
$$L_\gamma^{E_\gamma \geq 1\ \mathrm{GeV}} < 9.3 \times 10^{33}\ \mathrm{erg/s}. \tag{27}$$

The case of $\Gamma = 2$ will be discussed below.

The analysis of the pulsar PSR J1709 − 4429 did not reveal any sign of extended emission (see the lower panel of Fig. 4). The data give sawtoothed TS curves without any smooth peaks in all three energy ranges.

Note that an extended emission of size $R = 0.29° \pm 0.04°$ above 100 GeV around this pulsar has been detected by the HESS Collaboration [60]. In 3FGL the corresponding source is modeled as a point source, and our analysis shows that the extension seen by HESS is not resolved in the Fermi-LAT data. In any case, the angular extension of the HESS excess is very small and cannot be interpreted as a gamma-ray halo.

The TS curve for this pulsar in the energy bin 1–10 GeV lies systematically below the line $TS = 50$ for all halo radii. The scaling of TS with the halo flux (22) implies that the nonobservation of a halo at this significance can be translated into a bound on the corresponding flux,

$$TS_{1\text{–}10} < 50 \Rightarrow F^{1\text{–}10\ \mathrm{GeV}} < 3.0 \times 10^{-9}\ \mathrm{ph/cm^2\,s}. \tag{28}$$

Assuming the spectral index $\Gamma = 2.4$, this gives the following constraints:

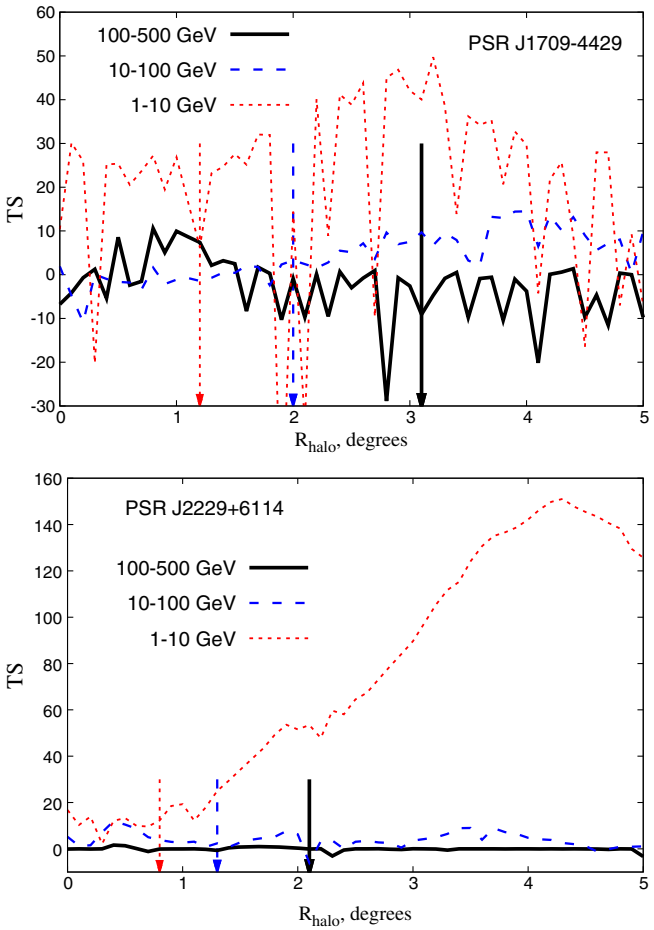

FIG. 4. $TS(R_{\rm halo})$ curves for PSR J1709 − 4429 (upper panel) and PSR J2229 + 6114 (lower panel). Vertical arrows show the sizes of the halos that are expected from the estimate (8).

$$F^{E_\gamma \geq 1\ \mathrm{GeV}} < 1.7 \times 10^{-11}\ \mathrm{erg/cm^2\,s},$$
$$L_\gamma^{E_\gamma \geq 1\ \mathrm{GeV}} < 1.4 \times 10^{34}\ \mathrm{erg/s}. \quad (29)$$

The results of our study for the pulsar PSR J2229 + 6114 are shown in the lower panel of Fig. 4. The TS curve above 100 GeV is almost flat and coincides with the $TS = 0$ axis. The TS curve in the range 10–100 GeV has a small insignificant peak at $R_{\rm halo} \approx 0.5°$ with the value $TS \approx 10$. In the range 1–10 GeV the TS curve features a slight enhancement over the range $R_{\rm halo} \approx 0.5 - 1°$ with $TS \sim 10$ and a significant peak at $R_{\rm halo} \approx 4.5°$ with $TS \sim 150$.

The extended emission of size 0.5° seen in the range 10–100 GeV likely corresponds to PWN G106.65 + 2.96 (associated with SNR G106.3 + 2.7; see Refs. [61,62]), whose counterpart was modeled as a point source in the 3FGL catalogue (and hence, in our source model). The latter accounts for the marginal improvement of TS when adding an extended template to the source model. We conclude that for a given pulsar the data do not show any evidence for extended emission which can be attributed to a gamma-ray halo.

The emission observed at $R \approx 4.5°$ might originate from the Galactic plane. In any case, such a large angular separation (which would correspond to ∼200 pc if projected at the pulsar's distance) implies that this emission is not related to the pulsar of interest.

Analogous to the previous pulsar, the fact that the TS curve for PSR J2229 + 6114 in the energy bin 1–10 GeV lies below the line $TS = 30$ at halo sizes $R_{\rm halo} \lesssim 1.5°$ can be used to put a bound on the halo luminosity,

$$TS_{1-10} < 30 \Rightarrow F^{1-10\ \mathrm{GeV}} < 2.0 \times 10^{-9}\ \mathrm{ph/cm^2\ s}. \quad (30)$$

Assuming the spectral index $\Gamma = 2.4$, this implies

$$F^{E_\gamma \geq 1\ \mathrm{GeV}} < 1.1 \times 10^{-11}\ \mathrm{erg/cm^2\,s},$$
$$L_\gamma^{E_\gamma \geq 1\ \mathrm{GeV}} < 1.2 \times 10^{34}\ \mathrm{erg/s}. \quad (31)$$

An important step in deriving the constraints on halo luminosities was the choice of the spectral index $\Gamma = 2.4$. The constraints, essentially, do not change under the assumption of harder spectra. Indeed, in this case one can constrain the halo luminosity by using the signal in the energy bin 10–100 GeV [see Eq. (22)]. For instance, having assumed the slope with $\Gamma = 2$ one can derive the following constraint for the PSR J2229 + 6114 case:

$$F^{1\ \mathrm{GeV} \leq E_\gamma \leq 500\ \mathrm{GeV}} < 1.8 \times 10^{-11}\ \mathrm{erg/cm^2\,s},$$
$$L_\gamma^{1\ \mathrm{GeV} \leq E_\gamma \leq 500\ \mathrm{GeV}} < 2.0 \times 10^{34}\ \mathrm{erg/s}, \quad (32)$$

which stays, essentially, at the same level as Eq. (31). Note that the difference between Eq. (31) and Eq. (32) can be used as an estimate for an error introduced by spectra extrapolations. We see that it brings ∼30% uncertainty.

B. Pulsars with compact halos

For the pulsar PSR J0205 + 6449 the data show no evidence of extended emission in all three energy bands (see the upper panel of Fig. 5). The TS curves lie around zero in the ranges 10–100 GeV and 100–500 GeV, while in the band 1–10 GeV the TS curve oscillates around a constant value $TS \approx 20$, which suggests that this offset resulted from inaccuracies in the background modeling.

The TS curve for the pulsar PSR J1357 − 6429 (see the lower panel of Fig. 5) is quite jagged above 100 GeV and has a wide peak with two small spikes at $R_{\rm halo} \approx 0.6°$ with the significance $TS \approx 20$. In the energy band 10–100 GeV the TS curve lies near the zero axis for $R_{\rm halo} \gtrsim 1°$ and features a small excess at $R_{\rm halo} \approx 0.3°$ with the maximum values $TS \approx 16$. The TS curve for 1–10 GeV lies around zero for almost all halo radii.

The excess above 100 GeV is likely associated with the extended HESS J1356-645 source [63,64], whose counterpart in the 3FGL catalogue (3FGL J1356.6 − 6428) is modeled as a point source. This explains the marginal

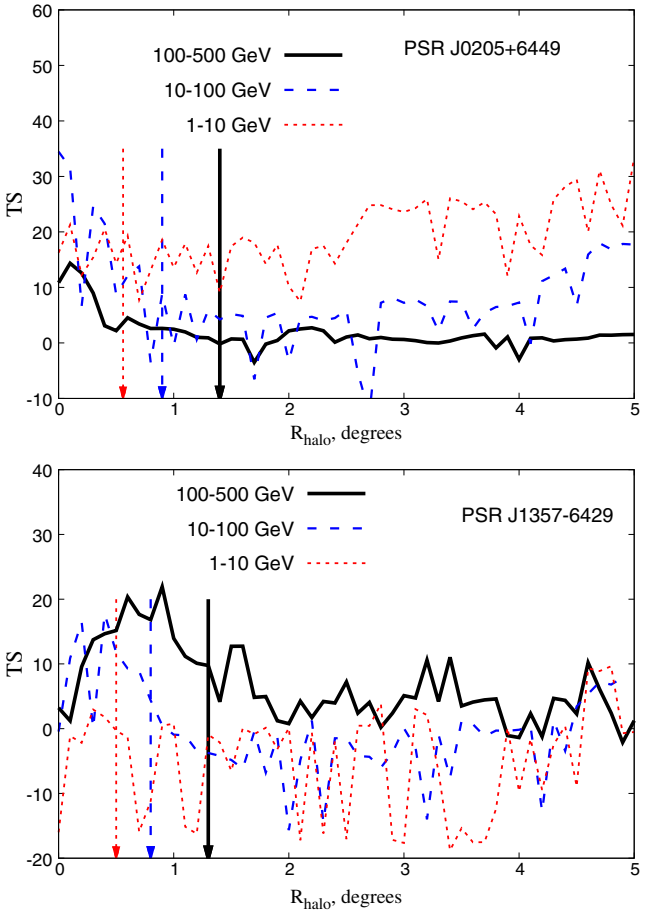

FIG. 5. $TS(R_{\rm halo})$ curves for PSR J0205 + 6449 (upper panel) and PSR J1357 − 6429 (lower panel). Vertical arrows show the sizes of the halos that are expected from the estimate (8).

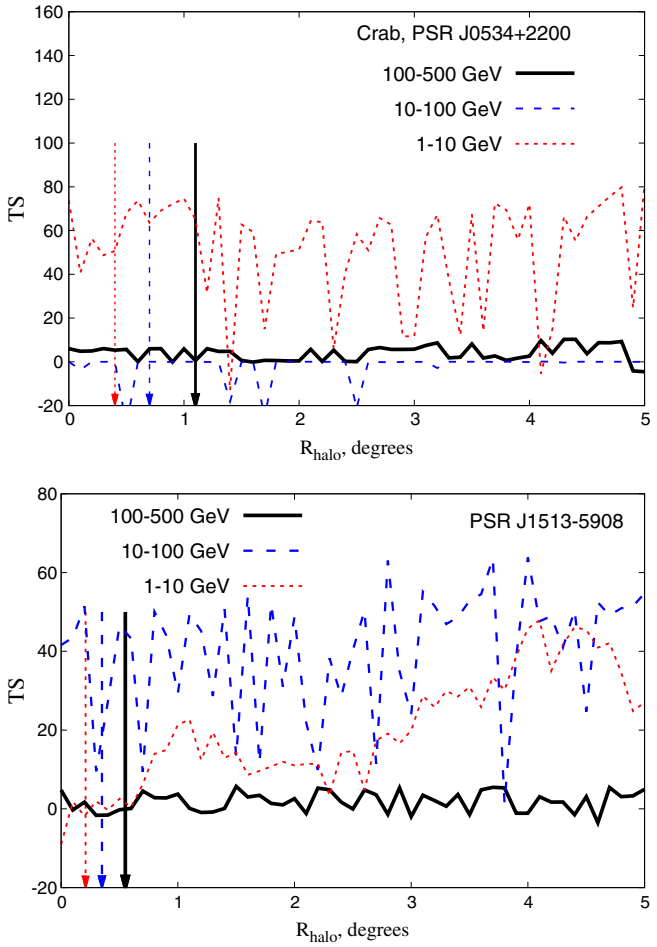

FIG. 6. $TS(R_{\rm halo})$ curves for Crab (PSR J0534 + 2200, upper panel) and PSR J1513 − 5908 (lower panel). Vertical arrows show the sizes of the halos that are expected from the estimate (8).

improvement of the TS achieved by adding an extended template of size $R_{\rm halo} \sim 0.5°$. The combination of radio, x-ray, and gamma-ray observations indicates that this source is a PWN, whose gamma emission has a leptonic origin [64].

On the other hand, we see that adding extended templates does not improve the TS significantly in the 1–10 GeV and 10–100 GeV bins, which indicates the absence of any evidence of a gamma-ray halo, at least at the present level of sensitivity.

The Crab Pulsar and Nebula are very bright gamma-ray sources in the Galaxy [65,66]. The Crab pulsar is also the youngest and the most energetic one from our sample, which is why it is most likely to feature a gamma-ray halo. However, contrary to expectations, the analysis of the Crab pulsar does not show any evidence of a gamma-ray halo in any energy bin (see the upper panel of Fig. 6). In the bins 10–100 and 100–500 GeV the TS curves essentially coincide with the $TS = 0$ axis. The TS curve at 1–10 GeV does not show any smooth peak and oscillates around a constant value $TS \sim 40$.

The observation of the pulsar PSR J1513 − 5908 (also known as PSR B1509 − 58) did not disclose any excess above 100 GeV (see the lower panel of Fig. 6). The TS curve in the range 10–100 GeV is very spiky and oscillates around a constant value $TS \simeq 30$ over the whole range of radii, which suggests that this offset is caused by uncertainties in background modeling. In the range 1–10 GeV the TS curve has two peak-like features at $R_{\rm halo} \approx 1°$ and $R_{\rm halo} \approx 4.5°$. These peaks are far from being smooth and most likely are caused by other sources in the Galactic plane. The pulsar of interest has rather low galactic latitude and adjoins many gamma-ray sources. E.g., the 5° region of interest contains at least four extended HESS sources of sizes $R \sim 0.1° - 0.3°$ which were modeled as point sources in 3FGL (HESS J1503 − 582, HESS J1458 − 608, HESS J1458 − 608, HESS J1507 − 622), and a collective effect can mimic an extended halo.

1. Constraints on halo luminosity

Let us discuss now the constraints on halo luminosities, which can be obtained from the subset of pulsars with compact halos. The most conservative bound can be derived by making use of the pulsar PSR J1513-5908.

The scaling of the TS with the halo flux [Eq. (22)] suggests that the nonobservation of a halo in the energy bin 10–100 GeV at significance $TS = 60$ can be translated into the upper limit on the halo flux,

$$TS_{10-100} < 60 \Rightarrow F^{10-100\ \mathrm{GeV}} < 4 \times 10^{-10}\ \mathrm{ph/cm^2\ s}. \tag{33}$$

Using the spectral index $\Gamma = 2.4$, this gives the constraints on the total flux and luminosity in the energy range $E_\gamma \geq 1$ GeV,

$$F^{E_\gamma \geq 1\ \mathrm{GeV}} < 5.8 \times 10^{-11}\ \mathrm{erg/cm^2\ s},$$
$$L_\gamma^{E_\gamma \geq 1\ \mathrm{GeV}} < 1.3 \times 10^{35}\ \mathrm{erg/s}, \tag{34}$$

which is 1 order of magnitude weaker than the bounds obtained for pulsars with large halos.

On the other hand, the strongest bound can be inferred from the Crab pulsar. Indeed, performing the same manipulations as above, one obtains

$$TS_{10-100} < 10 \Rightarrow L^{E_\gamma \geq 1\ \mathrm{GeV}} < 6.7 \times 10^{33}\ \mathrm{erg/s}. \tag{35}$$

The bounds on the luminosity for the rest of the pulsars with compact halos are scattered between those for Crab and PSR J1513 − 5908.

Notice that even the weakest bound (34) is roughly an order of magnitude smaller than the average luminosity of extended sources found in Ref. [18]. We will come back to this issue shortly.

VII. DISCUSSION

We found that only one pulsar (out of eight in our set) has extended gamma-ray emission which may be interpreted as a CR halo. Yet this interpretation is far from being definitive, which is why we stick to the constraints on halo luminosities obtained for other pulsars and relate them to the total energy of injected CRs.

We first focus on the pulsars with large halos. The constraints on the halo luminosity [cf. Eqs. (27), (29), (31), and (32)] are very similar for all of them, and can be written as

$$L_\gamma^{\mathrm{halo}} \lesssim (1-2) \times 10^{34}\ \mathrm{erg/s}. \tag{36}$$

The uncertainties induced by spectra extrapolations and inaccuracies in the scaling (22) contribute only ∼30% to the scatter in Eq. (36).

Using Eq. (10), the constraint (36) can be translated into a constraint on the total cosmic-ray energy,

$$\mathcal{E}_{\mathrm{CR}}^{\mathrm{halo}} \lesssim (0.5-1) \times 10^{50}\ \mathrm{erg}. \tag{37}$$

The above constraint implies that the total CR energy released by pulsars is still smaller than the benchmark mean value $\sim 2 \times 10^{50}$ erg required in order to produce the bulk of galactic CRs, although it hits the lower bound of Eq. (4). Thus, at face value, our results disfavor the scenario in which all galactic cosmic rays are injected in the ISM exclusively by newborn pulsars. We note that our result accords with recent studies which imply that the birth-period distribution of pulsars is close to log-normal with a mean value ∼100 ms [47,48]. This suggests that the rotational energy budget accessible for CR production should be typically smaller than 10^{50} erg [see Eq. (3)].

Before moving on we would like to comment more on the uncertainties in Eq. (37). First, one might worry about the diffusion coefficient D in Eq. (6), which is uncertain by a factor of 3 due to the degeneracy with the height of the galactic CR halo [32]. This coefficient enters the size of the diffusive halo with a square root in Eqs. (7) and (8), so that the uncertainly in its value is only $\sqrt{3} \simeq 1.7$. This uncertainly can affect our splitting into large and compact halos adopted in Sec. III by making the halos around the pulsars No 3 and 4 of Tables I and II compact, which calls for a reassessment of our constraints for these pulsars. If these pulsars are indeed the ones with compact halos one still can use the results in the energy bin 10–100 GeV [Eq. (32)], which are taken into account in the constraint (37). To sum up, the uncertainty related to the diffusion constant appears to not be crucial for our analysis.

The second, and more serious source of degeneracy is the interstellar matter density, which explicitly affects the constraint (37) through Eq. (10). Unfortunately, the measurements of density in the vicinity of pulsars are quite uncertain. For the pulsars of interest the average ISM density lies in the range $0.3 - 1\ \mathrm{cm^{-3}}$ [45], which translates to the following scatter:

$$\mathcal{E}_{\mathrm{CR}}^{\mathrm{halo}} \lesssim (0.5-3) \times 10^{50}\ \mathrm{erg}. \tag{38}$$

Our constraint now has an overlap with the energy required to account for all CRs exclusively with pulsars [Eq. (4)]. We point out, however, that the lower bound in Eq. (4) is a conservative value which should be taken with a grain of salt since it corresponds to a very high pulsar birthrate of $1/30\ \mathrm{yr^{-1}}$. To sum up, the degeneracy between $\mathcal{E}_{\mathrm{CR}}^{\mathrm{halo}}$ and n_{ISM} does not allow us to definitely rule out pulsars as main sources of CRs, but our analysis indicates appreciable tension in this scenario.

As for the extended halo observed around PSR J0007 + 7303, one might, in principle, interpret this gamma-ray emission as a counterpart of a CR halo. In that case, comparing the luminosity of this halo (25) with Eq. (10) and using the density $n_{\mathrm{ISM}} = (0.05\text{–}0.1)\ \mathrm{cm^{-3}}$ [46], one can estimate the related energy budget of CRs,

$$\mathcal{E}_{\mathrm{CR}}^{\mathrm{halo}} \sim (2-4) \times 10^{50}\ \mathrm{erg}. \tag{39}$$

Two comments are in order here. First, the interpretation of extended emission around PSR J0007 + 7303 as a SNR

or PWN is not ruled out at the moment. Thus, the value given in Eq. (39) should be considered as a conservative upper bound, since by having accounted for the presence of a SNR and PWN one will inevitably get a stronger constraint. Second, the emission in the energy bin 1–10 GeV can also be produced by electrons or positrons via inverse Compton scattering. The halo's angular radius projected at the pulsar's distance yields the physical halo size ∼30 pc, which implies that the lepton contribution can be quite significant at such small distances from the source. In order to clarify the situation an additional multiwavelength analysis of this halo is needed.

Now we discuss the subpopulation of pulsars with compact halos, which are younger and more energetic than the four we discussed above. Since the halo sizes are expected to be quite small for these pulsars, their observation with LAT becomes challenging given its limited resolution at small angular scales. That is why we expect the constraints on CR power to degrade if the analysis is based only on the youngest pulsars. The bounds on the halo luminosity (34)–(35) can be related to the total energy of CRs via Eq. (10),

$$\mathcal{E}_{\rm CR}^{\rm halo} \lesssim (0.3-7)\times 10^{50}\ {\rm erg}. \tag{40}$$

The range is quite wide in this case and, if we used only the subpopulation of pulsars with compact halos, the scenario in which all CRs in the Galaxy are born by pulsars would be largely unconstrained.

One might notice the apparent tension between our results and the detection of gamma-ray halos above 100 GeV with average fluxes $\sim 5\times 10^{-11}$ erg/cm^2 s reported in Ref. [18]. These fluxes yield the typical halo luminosity above 1 GeV $\sim 5\times 10^{35}$ erg/s [see Eq. (13)], significantly exceeding our bounds. There are several ways to explain this tension.

On the one hand, the extended halos observed in Ref. [18] may be spurious, i.e., produced by background fluctuations or projection effects. With the new Fermi-LAT data we checked that the *N-S* emission is not due to background fluctuations (see Appendix C for details). The interpretation of *N-S* halos as a projection effect of several independent VHE sources, however, cannot be excluded, and moreover seems plausible given that all the *N-S* sources are located in the Galactic plane.

On the other hand, the halos observed in Ref. [18] can be produced by a mechanism involving multiple sources, such as the interaction between pulsars, SNRs, and the interstellar medium. In such a case these halos can exist only in a specific environment and there is little hope to find them in each sample of young pulsars. This explanation is supported by the fact that most of the *N-S* sources were found in the Norma arm of the Galaxy, which is known as a peculiar region with the highest star-formation rate and an average gas density $n_{\rm ISM}\sim 10$ cm^{-3} [67]. The high density of the ISM and the presence of molecular clouds can significantly boost the luminosity of extended halos even with the CR input satisfying Eq. (37), which can readily resolve the tension. It should be stressed that "boosted luminosity" does not mean an increase in total energy, i.e., pulsars still cannot be the main source of CRs. More studies of the *N-S* sources in other frequency bands are needed in order to further clarify the situation.

Our analysis disfavors the pulsar origin of the bulk of galactic CRs, but it does not pin down the scenario in which pulsars produce only very energetic CRs with $E_{\rm CR}\gtrsim 100$ GeV, while other mechanisms are responsible for particle acceleration at lower energies. This scenario may well be true in the light of new evidence that the interstellar CR spectrum has multiple components [7,8]. This scenario can also reconcile the mentioned tension with Ref. [18] since our constraints are, essentially, based on the events in the energy range 1–10 GeV, which should be mostly due to CRs with $E_{\rm CR}\lesssim 100$ GeV, though in this case the spectral shape of CRs produced in pulsars should be rather specific.

Our analysis may be extended in several ways. One can further investigate the extended emission that we observed around PSR J0007 + 7303/SNR CTA1, and test it for signatures of CR production. Another way to go is to study in detail the nature of the extended emission found in Ref. [18]. As discussed, this requires proper accounting for VHE sources in their vicinity, and the use of other energy bands and neutrino signals [26]. Also it will be interesting to update our analysis once more data are accumulated, e.g., with the new gamma-ray telescopes such as CTA or HAWC [68,69].

VIII. CONCLUSIONS

In this paper we scrutinized the hypothesis that galactic CRs are produced by pulsars at birth. In order to account for the bulk of the galactic CRs it is sufficient that their sources release some $\sim 2\times 10^{50}$ erg energy every ∼50 years in the form of CRs. This power can be, in principle, generated by the rotational energy of neutron stars right after supernova explosions. If this is the case, CRs should interact with the interstellar medium as they escape from their parent pulsars and thus produce gamma radiation observable as extended halos. The observations of these halos can be used in order to estimate the total energy of injected CRs.

In this study we sought gamma-ray halos around young pulsars in the recent 7-year Fermi-LAT data. Using the Pass 8 reconstruction and statistical tools provided by the LAT Collaboration, we tested a specially selected sample of pulsars whose hypothetical gamma-ray halos could be unambiguously identified. As a result, we found only one extended source which can be interpreted as a gamma-ray counterpart of a CR halo. This is the one-degree halo around the pulsar PSR J0007 + 7303 detected in the energy bin 1–10 GeV. The overall luminosity of the

halo above 1 GeV is $\sim 3 \times 10^{33}$ erg/s, which implies the total energy of corresponding CRs $\sim 2 \times 10^{50}$ erg. We emphasize that the other interpretations of this emission are not excluded and further studies of this source are required.

Without any assumptions on the nature of this emission we derived a constraint on the typical luminosities of gamma-ray halos, $L_{\rm halo} \lesssim 10^{34}$ erg/s. This implies that the total energy of CRs produced by a pulsar at birth should typically be smaller than 10^{50} erg, and thus disfavors the scenario in which galactic CRs are produced entirely by pulsars. There are possible caveats in the interpretation of our result. First, our constraints are quite degenerate with the ISM density. Second, there is large uncertainty in the expected pulsar CR luminosity due to current imperfect knowledge of pulsar birthrates.

ACKNOWLEDGMENTS

We thank M. Libanov, S. Sibiryakov, B. Nizamov, S. Troitsky, and V. Vasiliev for useful discussions. We thank K. Postnov for pointing out the references on the initial periods of pulsars, and for helpful and encouraging comments. We are grateful to A. Neronov and D. Semikoz for their valuable comments on the draft. We also thank the referee for a thorough report which has substantially improved the presentation. The authors acknowledge the support by the Russian Science Foundation Grant No. 14-12-01340. The analysis is based on the data and software provided by the Fermi Science Support Center (FSSC). The numerical part of the work has been performed at the cluster of the Theoretical Division of INR RAS. During the work on this paper the authors were using the SIMBAD database and the ATNF pulsar database.

APPENDIX A: *N-S* PULSARS AND THEIR PROPERTIES

The *N-S* pulsars (those listed in Table II of Ref. [18]) and their characteristics are displayed in Table III.[5] In order to check that our set of pulsars belongs to the same population as the *N-S* pulsars, we first imposed a cut $T_{\rm SD} < 30$ kyr which selected 9 pulsars out of 15 present in Table III. Then we applied the two-sample KS test for a selected set of *N-S* pulsars and our set (see Table I). We performed this test for the distributions over $\dot{E}$ and P separately, and found the following p-values for either case:

$$p_{\rm KS}(\dot{E}) = 0.84,$$
$$p_{\rm KS}(P) = 0.62. \quad \text{(A1)}$$

TABLE III. The pulsars coincident with the extended sources in Ref. [18].

PSR	l	b	r_s, kpc	$T_{\rm SD}$, kyr	$\dot{E}$, erg/s	P, s
B1800-21	8.40	0.15	4.40	15.8	2.2×10^{36}	0.13
B1823-13	18.00	−0.69	4.12	21.4	2.8×10^{36}	0.10
J1838−0655	25.25	−0.20	6.60	22.7	5.5×10^{36}	0.07
J1841−0524	27.02	−0.33	4.89	30.2	1.0×10^{35}	0.44
J1856+0245	36.01	0.06	10.29	20.6	4.6×10^{36}	0.08
J2021+4026	78.23	2.09	2.15	76.9	1.2×10^{35}	0.26
J1023−5746	284.17	−0.41	$*$	4.6	1.1×10^{37}	0.11
J1420−6048	313.54	0.23	7.65	13	1.0×10^{37}	0.068
J1614−5144	331.62	−0.58	9.56	3270	8.1×10^{31}	1.5
J1617−5055	332.50	−0.28	6.46	8.13	1.6×10^{37}	0.069
J1632−4757	336.30	0.08	6.96	24	5.0×10^{34}	0.23
J1648−4611	339.44	−0.79	5.71	110	2.1×10^{35}	0.16
J1702−4128	344.74	0.12	5.18	55.1	3.4×10^{35}	0.18
J1708−4008	346.48	0.04	3.80	8.9	5.8×10^{32}	11.0
B1830−08	23.39	0.06	4.50	147	5.8×10^{35}	0.085

APPENDIX B: SIMULATIONS OF GAMMA-RAY HALOS

In this appendix we discuss in detail the simulations performed in order to better understand the potential signal. We chose to simulate the pulsar No 1 (PSR J0007 + 7303) for pulsars with large halos and the pulsar No 8 (PSR J1513 − 5908) for pulsars with compact halos.

The pulsar PSR J0007 + 7303 is very close and its galactic latitude is rather high ($b \sim 10°$), which results in a very low density of the LAT gamma-ray sources in the 10° RoI around this pulsar (there are only 22 sources). This pulsar thus represents the most clear case for our study. As discussed above, the hypothetical halo around this pulsar should have very large angular extension; see Table II.

On the other hand, the pulsar PSR J1513 − 5908 is pretty far away and located close to the Galactic plane. Apart from the pulsar itself, there are 51 other LAT sources in the corresponding 10° RoI. The pulsar of interest is very young ($T_{\rm SD} \sim 1$ kyr) and has a significant energy loss rate ($\dot{E} \sim 10^{37}$ erg/s). The halo around this pulsar should be quite small; see Table II.

To generate the Fermi-LAT events we made use of the *gtobssim* utility. For either pulsar we simulated events in the energy range 1–500 GeV for the relevant time interval (361 weeks) in the 10° RoI around the pulsar. The input model included all the LAT point and extended sources located within the RoI, the galactic and isotropic background, and the gamma-ray halo around the chosen pulsar. Spectral parameters and photon fluxes for the 3FGL sources were taken directly from the 3FGL catalogue, and the recommended values were chosen for the isotropic and galactic background fluxes.[6]

[5]Notice that the pulsar PSR J1708 − 4008 is incorrectly written in Table II of Ref. [18] as PSR J1706 − 4009.

[6]http://fermi.gsfc.nasa.gov/ssc/data/analysis/scitools/help/gtobssim.txt.

As discussed in Sec. V, for either pulsar we simulated two types of halos: the *bright* one and the *faint* one. For the bright halos [case *(a)* in what follows] we assumed the fluxes of order (11) in the energy bin 100–500 GeV. Having fixed the flux in the range 100–500 GeV [Eq. (11)] and assuming a simple power-law spectrum of a halo, $dN/dE = A_0 \times E^{-\Gamma}$, we computed the normalization factor A_0 for two particular choices of the spectral index: $\Gamma = 2.4$ and $\Gamma = 2$. This yielded the halo fluxes in the energy bands 1–10 GeV and 10–100 GeV.

In the case of a bright halo around the pulsar PSR J1513 − 5908 we fixed the flux (11) at $r_s = 4.4$ kpc in the energy bin 100–500 GeV and extrapolated the spectrum down to 1 GeV as discussed above. The results are shown in the two right columns of Table IV. For the pulsar PSR J0007 + 7303, in fact, the straightforward substitution $r_s = 1.4$ kpc in Eq. (11) yielded a very high flux value. The halo appeared to be so bright that it drastically deteriorated the convergence of our likelihood optimization procedure. In order to facilitate the numerical analysis for this pulsar, we reduced the flux 4 times compared to the one extracted directly from Eq. (11). The resulting fluxes are listed in Table V.

In the case of faint halos [case *(b)* in what follows] we were looking for typical fluxes that yield the detection at $TS \sim 100$ in one of the energy bins.

For PSR J1513 − 5908 we found that the flux 10^{-9} ph/cm^2 s in the energy bin 10–100 GeV gives the halo detection at $TS \sim 120$. Having fixed the flux in this range, we derived the fluxes at 1–10 GeV and 100–500 GeV for spectra with $\Gamma = 2.4$ and $\Gamma = 2$. The results are listed in the two right columns of Table VI.

In the case of PSR J0007 + 7303 we found that the flux 5×10^{-9} ph/cm^2 s in the energy bin 1–10 GeV leads to halo detection at $TS \sim 100$ in this range. Then, having fixed the flux at 1–10 GeV and assuming a power-law spectrum with indices $\Gamma = 2.4$ and $\Gamma = 2$, we computed the fluxes in the bins 10–100 and 100–500 GeV. The results are shown in the two right columns of Table VII.

Given the power-law distribution of photons, most of them "sit" at the lower boundary of each energy bin. Thus, it is natural to assume that the angular size of the halo within each narrow energy bin is constant and defined by the lower energy of the bin.[7] In that way, we computed the sizes of the gamma-ray halos in the energy bins 1–10, 10–100, and 100–500 GeV by plugging the values $E_\gamma = 1$, 10, 100 GeV, correspondingly, into Eq. (8). The obtained angular sizes of the gamma-ray halos for relevant energy ranges are listed in the second columns of Tables V, IV, VII, and VI.

[7]In fact, the photons with higher energy have greater statistical significance. However, this subtlety is not crucial for our further analysis given other uncertainties in the estimate (8).

TABLE IV. Fluxes (in photons/cm^2/s) and angular sizes of the simulated *bright* gamma-ray halo around the pulsar PSR J1513 − 5908 for different energy bands and spectral indices.

E, GeV	$R_{\rm halo}$	F, cm^{-2} s^{-1} [$\Gamma = 2.4$]	F, cm^{-2} s^{-1} [$\Gamma = 2$]
100–500	0.6°	2.2×10^{-10}	2.0×10^{-10}
10–100	0.4°	5.8×10^{-9}	2.2×10^{-9}
1–10	0.2°	1.5×10^{-7}	2.2×10^{-8}

TABLE V. Fluxes (in photons/cm^2/s) and angular sizes of the simulated *bright* gamma-ray halo around the pulsar PSR J0007 + 7303 for different energy bands and spectral indices.

E, GeV	$R_{\rm halo}$	F, cm^{-2} s^{-1} [$\Gamma = 2.4$]	F, cm^{-2} s^{-1} [$\Gamma = 2$]
100–500	5.0°	5.0×10^{-10}	5.0×10^{-10}
10–100	3.2°	1.4×10^{-8}	5.6×10^{-9}
1–10	2.0°	3.4×10^{-7}	5.6×10^{-8}

TABLE VI. Fluxes (in photons/cm^2/s) and angular sizes of the simulated *faint* gamma-ray halo around the pulsar PSR J1513 − 5908 for different energy bands and spectral indices.

E, GeV	$R_{\rm halo}$	F, cm^{-2} s^{-1} [$\Gamma = 2.4$]	F, cm^{-2} s^{-1} [$\Gamma = 2$]
100–500	0.6°	3.7×10^{-11}	1.0×10^{-10}
10–100	0.4°	1.0×10^{-9}	1.0×10^{-9}
1–10	0.2°	2.5×10^{-8}	1.0×10^{-8}

TABLE VII. Fluxes (in photons/cm^2/s) and angular sizes of the simulated *faint* gamma-ray halo around the pulsar PSR J0007 + 7303 for different energy bands and spectral indices.

E, GeV	$R_{\rm halo}$	F, cm^{-2} s^{-1} [$\Gamma = 2.4$]	F, cm^{-2} s^{-1} [$\Gamma = 2$]
100–500	5.0°	7.4×10^{-12}	4.44×10^{-11}
10–100	3.2°	2.0×10^{-10}	5.0×10^{-10}
1–10	2.0°	5.0×10^{-9}	5.0×10^{-9}

The gamma-ray halo was inserted into the *gtobssim* source models for both pulsars as three uniformly bright circles of sizes and fluxes given in Tables V, IV, VII, and VI, such that the flux of each template was restricted to the corresponding energy band and was put to zero everywhere else. Within each band the photons were distributed over the power law with the corresponding index Γ.

After generation, the simulated events were processed using the *gtlike* utility analogous to the real data (see Sec. IV).

The results of the analysis for the simulated bright gamma-ray halo around PSR J0007 + 7303 are shown in Fig. 7. We see that the *gtlike* utility is more biased towards smaller halo sizes than the simulated ones, which indicates that the likelihood optimization procedure prefers halos with larger surface brightness. The bias is quite strong

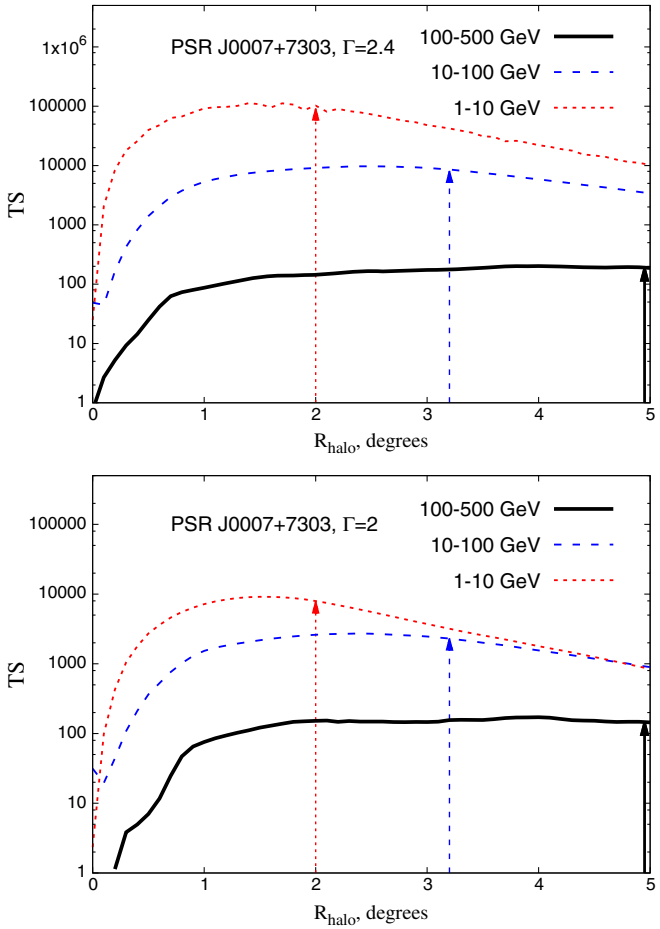

FIG. 7. $TS(R_{\rm halo})$ curves for the simulated *bright* gamma-ray halo around the pulsar PSR J0007 + 7303 for the spectral indices $\Gamma = 2.4$ (upper panel) and $\Gamma = 2$ (lower panel). The results of the analysis in different energy bands are shown as a black solid line for 100–500 GeV, a blue dashed line for 10–100 GeV, and a red dotted line for 1–10 GeV. Vertical arrows show the sizes of the halos that were input into the simulations.

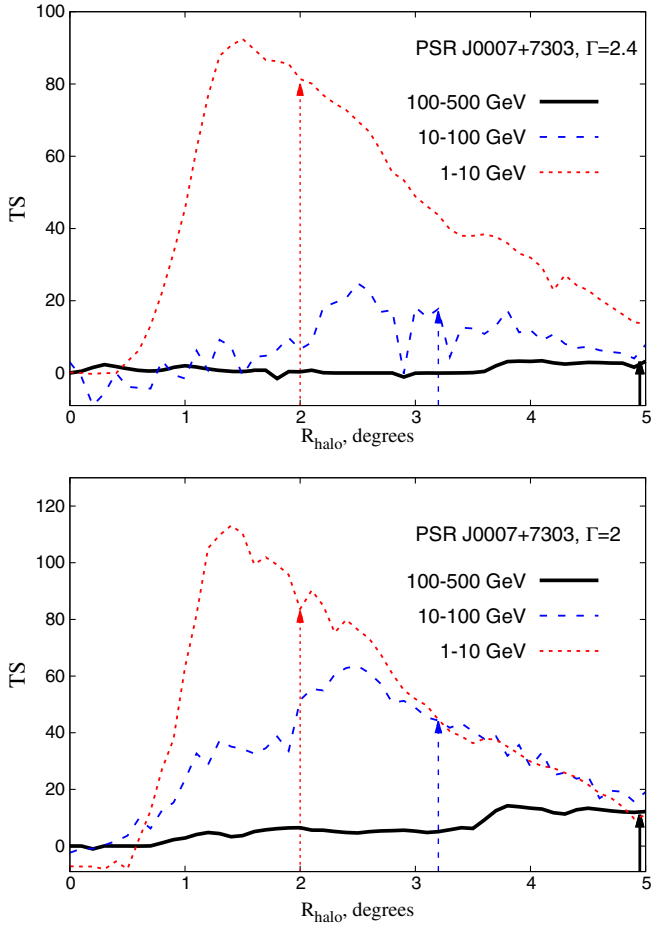

FIG. 8. $TS(R_{\rm halo})$ curves for the simulated *faint* gamma-ray halo around the pulsar PSR J0007 + 7303 for the spectral indices $\Gamma = 2.4$ (upper panel) and $\Gamma = 2$ (lower panel). The results of the analysis in different energy bands are shown as a black solid line for 100–500 GeV, a blue dashed line for 10–100 GeV, and a red dotted line for 1–10 GeV. Vertical arrows show the sizes of the halos that were inserted into the simulations.

above 100–500 GeV (where less events are present) and weakens at lower energies which contain more statistics. In the bin 100–500 GeV the TS curve flattens already at $R_{\rm halo} \simeq 2°$ and turns into a plateau with $TS \sim 160$. In the other energy bins (1–10 and 10–100 GeV) the TS curves also become flat rather fast and after that have very moderate dependence on $R_{\rm halo}$.

The behavior is similar in the case of the faint gamma-ray halos around PSR J0007 + 7303 (see Fig. 8), where one can still see a small offset between the sizes of simulated and observed halos. Note that even in the case of a faint halo, the detection with significance $TS \simeq 20$ ($TS \simeq 60$) is possible in the energy bin 10–100 GeV for the power-law index $\Gamma = 2.4$ ($\Gamma = 2$). The significance in the range 100–500 GeV is very small, which means that a halo is practically undetectable in this bin.

The results of our analysis of the bright halo around PSR J1513 − 5908 for the spectral indices 2 and 2.4 are displayed in Fig. 9. The small size of the halo with respect to LAT PSF results in a relatively small statistical significance of the halo at energies 1–10 GeV. We found, again, a small bias between the simulated and detected sizes of the halo at energies above 10 GeV. This bias is, however, not as strong as the one we saw in the PSR J0007 + 7303 case. Given that for either spectral index we fixed the same flux above 100 GeV, the signal is very similar in this energy range and has $TS \sim 40$ for either spectrum. The excess in the energy bin 10–100 GeV is quite significant in either case.

The signal in the energy bin 1–10 GeV is quite different depending on the spectral index. A soft spectrum with $\Gamma = 2.4$ implies a larger signal in the energy bin 1–10 GeV, which has the same TS as the signal at 10–100 GeV (see the upper panel of Fig. 9). On the other hand, a harder spectrum with $\Gamma = 2$ implies a rather faint signal in the energy bin 1–10 GeV.

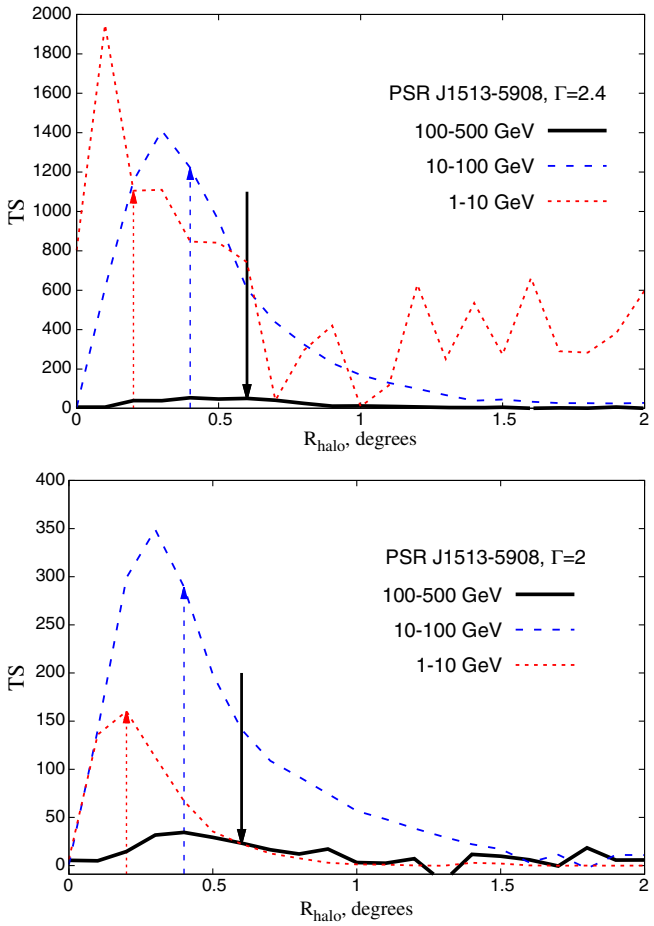

FIG. 9. $TS(R_{\rm halo})$ curves for the simulated *bright* halo around the pulsar PSR J1513 − 5908 for the spectral indices $\Gamma = 2.4$ (upper panel) and $\Gamma = 2$ (lower panel).

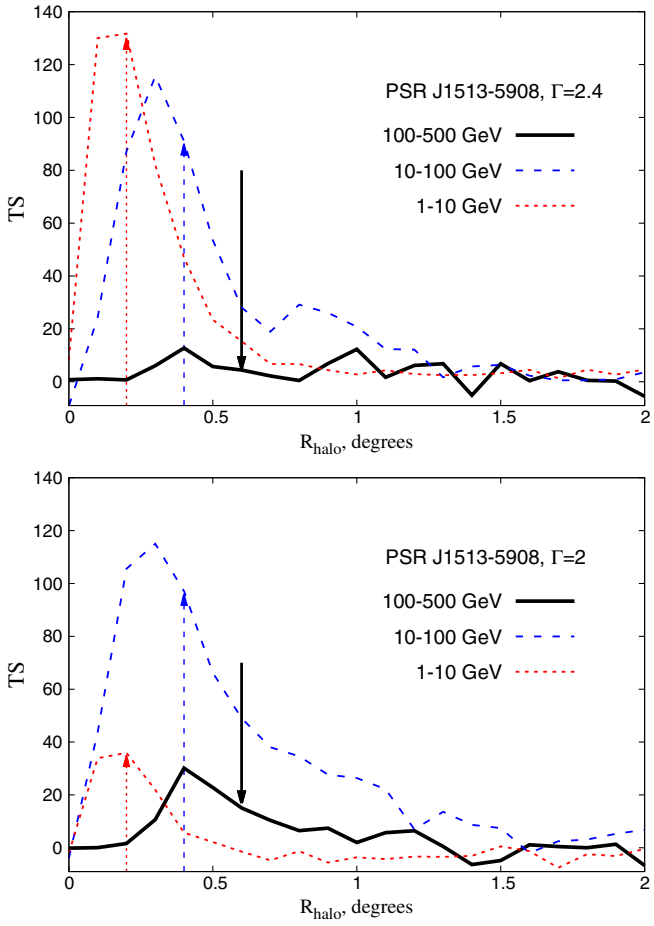

FIG. 10. $TS(R_{\rm halo})$ curves for the simulated *faint* halo around the pulsar PSR J1513-5908 for the spectral indices $\Gamma = 2.4$ (upper panel) and $\Gamma = 2$ (lower panel).

The results of our analysis for the faint halo around PSR J1513-5908 are displayed in Fig. 10. Since we fixed the flux in the energy bin 10–100 GeV, the signal depends drastically upon the spectral index. If the halo is observed at $TS \sim 100$ in the energy range 10–100 GeV, then one may expect a signal with similar significance at 1–10 GeV in the case of soft spectra (see the upper panel of Fig. 10 for $\Gamma = 2.4$). In the case of hard spectra ($\Gamma = 2$, lower panel of Fig. 10) the signal is observed in both the 1–10 GeV and 100–500 GeV bins with similar significance $TS \sim 40$.

1. TS-flux scaling

In order to put constraints on the halo luminosity we studied the dependence of test statistics for halos upon their fluxes (or, equivalently, the number of photons). We sampled ∼10 halo flux values for each energy bin and generated events for these fluxes with *gtobssim*. As above, we assumed two choices for the spectral index: $\Gamma = 2$ and $\Gamma = 2.4$. Then we processed these events with *gtlike* and took corresponding TS values from the maximums of the obtained TS curves.

Let us first discuss the case of PSR J0007 + 7303. In the upper panel of Fig. 11 we show our results for $\Gamma = 2$. Assuming the ansatz $TS = aF^b$ we obtained the following scaling:

$$\begin{aligned} TS_{1\text{–}10} &\simeq 100\left[\frac{F^{1\text{–}10\ \mathrm{GeV}}}{4.6\times10^{-9}\ \mathrm{ph/cm^2\,s}}\right]^{b_1}, \\ b_1 &= 1.54 \pm 0.06, \\ TS_{10\text{–}100} &\simeq 100\left[\frac{F^{10\text{–}100\ \mathrm{GeV}}}{5.7\times10^{-10}\ \mathrm{ph/cm^2\,s}}\right]^{b_2}, \\ b_2 &= 1.42 \pm 0.14, \\ TS_{100\text{–}500} &\simeq 100\left[\frac{F^{100\text{–}500\ \mathrm{GeV}}}{2.4\times10^{-10}\ \mathrm{ph/cm^2\,s}}\right]^{b_3}, \\ b_3 &= 1.33 \pm 0.10. \end{aligned} \tag{B1}$$

For the case of $\Gamma = 2.4$ we found, essentially, the same scaling as Eq. (B1); see the lower panel of Fig. 11. For the 1–10 GeV bin we have

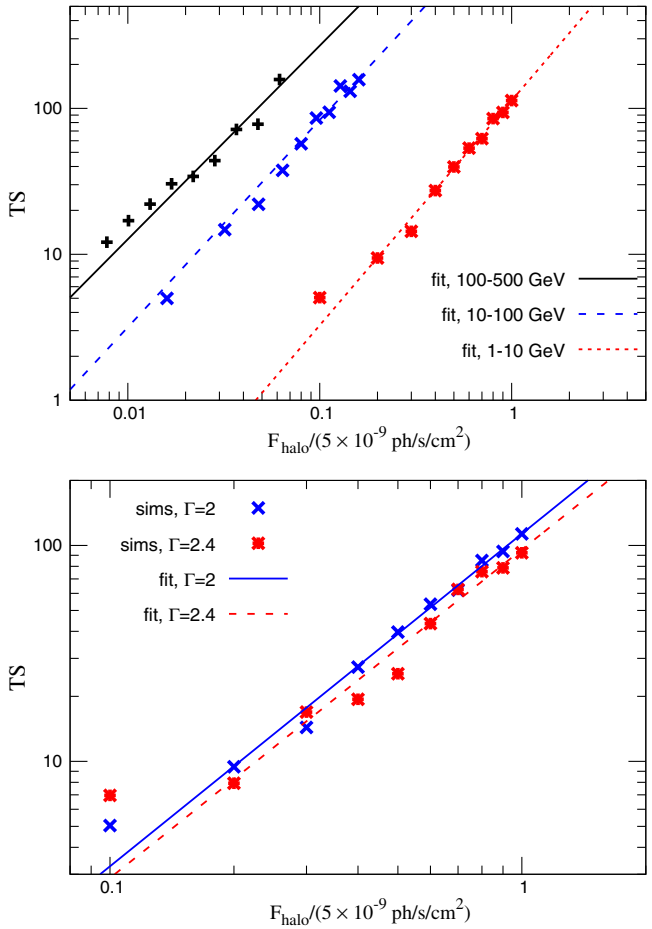

FIG. 11. The $TS(F_{\rm halo})$ dependence retrieved from simulations. Upper panel: Results for different energy bins for $\Gamma = 2$. Lower panel: The dependence for different spectral indices for the energy bin 1–10 GeV. All curves are measured for PSR J0007 + 7303.

$$TS_{1-10}^{\Gamma=2.4} \simeq 100\left[\frac{F^{1-10\ \rm GeV}}{5.1\times10^{-9}\ \rm ph/cm^2\,s}\right]^{b'},$$
$$b' = 1.52 \pm 0.13. \qquad \text{(B2)}$$

We also found that in each energy bin this scaling depends on the background flux (galactic interstellar and isotropic emission), but this dependence is very mild and can notably affect the scaling only for extreme values, which are ruled out by observations.

As for the case of PSR J1513 − 5908, in the energy bins 10–100 and 100–500 GeV we found almost the same scaling as that for PSR J0007 + 7303, while the scaling in the energy bin 1–10 GeV is very different from that obtained in Eq. (B1). For instance, in order to detect a halo in this energy bin at $TS = 100$ one requires the flux $F^{1-10\ \rm GeV} \sim 2\times10^{-8}$ ph/cm^2 s, which is 25 times bigger than the analogous flux in the case of PSR J0007 + 7303.

On the other hand, the scaling at energies above 10 GeV is essentially the same for both pulsars, which suggests that if the angular size of a halo is larger than the LAT PSF, the scaling of halo test statistics with the flux in each energy bin is a generic property which is valid for any source and can be used to derive constraints from the data.

We additionally simulated a faint halo around the pulsar PSR J1709 − 4429 and found, up to a few percent difference, the same TS dependence on the flux as Eq. (B1). We also performed additional checks to verify that the scaling (B1) is valid with accuracy $\lesssim$20% in the region of interest $TS \sim 50$ for the energy bins 1–10 and 10–100 GeV for various spectral indices and background fluxes.

Overall, our analysis implies that in the energy bins 10–100 and 100–500 GeV the scaling is given by Eq. (B1) and is valid for both subpopulations. The scaling in the energy bin 1–10 GeV [Eq. (B1)] is generic only for the pulsars with large halos.

APPENDIX C: FLUCTUATIONS OR NOT?

In Ref. [18] the LAT events above 100 GeV from August 2008 to October 2011 were analyzed using the minimal spanning tree method. Then only the halos coincident with known sources from the TeVCat catalogue were selected for further analysis. This procedure, however, does not guarantee that the N-S sources selected in that way are not due to background fluctuations. In this section we perform an independent check to make sure that this is not the case.

For each source listed in Table II of Ref. [18] we computed the expected number of photons in the time

TABLE VIII. For each extended source of Ref. [18] we display $N_{\rm exp}$ [the expected number of photons in the time span October 2011–July 2015 computed using Eq. (C1)], $N_{\rm obs}$ (the observed number of photons), $N_{2008-2011}$ (the number of photons observed in the span August 2008–October 2011), and p-val (the Poissonian p-values corresponding to the probability to observe $N \leq N_{\rm obs}$ events expecting $N_{\rm exp}$).

N-S source	$N_{\rm exp}$	$N_{\rm obs}$	$N_{2008-2011}$	p-val
1	28.161	29	20	0.611
2	30.606	27	22	0.294
3	76.535	63	55	0.065
4	24.820	23	18	0.408
5	42.622	37	31	0.219
6	20.560	25	15	0.861
7	5.391	7	4	0.823
8	6.984	7	6	0.601
9	8.281	7	7	0.414
10	13.017	5	11	0.011
11	12.476	11	10	0.408
12	27.747	34	21	0.897
13	23.871	39	18	0.998
14	40.240	40	30	0.527
15	33.771	21	25	0.013
16	39.861	34	29	0.200
17	19.229	15	14	0.200
18	15.502	11	11	0.154

span October 2011–July 2015 inside the circles corresponding to the halo sizes (θ_{90} from Ref. [18]). For each source we assumed the fluxes as retrieved from the data part August 2008–October 2011, which was used in Ref. [18]. This yielded the following expected number of photons:

$$N_{\rm exp} = N_{2008\text{–}2011}\frac{\mathcal{E}_{2011\text{–}2015}}{\mathcal{E}_{2008\text{–}2011}}, \quad \text{(C1)}$$

where $N_{2008-2011}$ is the number of photons observed inside the θ_{90} circles from August 2008 to October 2011, and by $\mathcal{E}$ we denote the exposition for the relevant time span. Notice that in Table II of Ref. [18] N_{ph} is the background subtracted number of photons. The number $N_{2008-2011}$ we present here also includes the background ones.

Having computed the expected number of photons we compared them to $N_{\rm obs}$, the observed numbers of photons in the time span October 2011–July 2015 inside the same halos. The results are shown in Table VIII. For each source we computed the p-values corresponding to the Poissonian probability to observe $N \leq N_{\rm obs}$ events expecting $N_{\rm exp}$. The p-values are compatible with our null hypothesis, that is, the N-S sources have stable fluxes and are not produced by fluctuations.

APPENDIX D: 3FGL SOURCES

In this appendix we show the best-fit results for 3FGL sources within our 10° RoI for the 1–10 GeV bin for PSR J0007 + 7303. Corresponding parameters are listed in Table IX. The best fits for other extended models can be obtained upon request at mikhail.ivanov@cern.ch. For source model definitions see Ref. [70].

TABLE IX. Results of the *gtlike* fit for the model that includes a 1.1° uniform halo around PSR J0007 + 7303. Benchmark values from the 3FGL catalogue are presented for comparison. The benchmark value for the normalization of galactic and isotropic emissions is 1.

3FGL name	Model and parameters	Parameters, 3FGL	Parameters with halo	Distance, °
J0007.0 + 7302	PLSuperExpCutoff, (E_c(MeV), $N_0 \times 10^{10}$, γ_1)	1732, 1.45, −1.208	1734 ± 10, 1.3464 ± 0.0067, -1.1860 ± 0.0048	0.0
J0012.4 + 7040	PowerLaw, ($N_0 \times 10^{13}$, γ)	5.5, −2.48	Removed ($TS < 5$)	2.41
J0028.6 + 7507	PowerLaw, ($N_0 \times 10^{13}$, γ)	5.04, −2.34	5.00 ± 0.44, -2.32 ± 0.09	2.54
J2355.4 + 6939	PowerLaw, ($N_0 \times 10^{13}$, γ)	6.62, −2.54	Removed ($TS < 5$)	3.52
J0008.5 + 6853	LogParabola ($N_0 \times 10^{12}$, α, β)	4.26, 2.42, 0.93	1.96 ± 0.19, 2.11 ± 0.10, 0.403 ± 0.072	4.16
J2356.9 + 6812	PowerLaw, ($N_0 \times 10^{12}$, γ)	1.67, −2.63	1.14 ± 0.17, -2.77 ± 0.14	4.90
J0004.2 + 6757	PowerLaw, ($N_0 \times 10^{13}$, γ)	6.01, −2.49	7.13 ± 0.75, -4.35 ± 0.46	5.09
J2353.3 + 6639	LogParabola ($N_0 \times 10^{12}$, α, β)	9.12, 2.45, 0.999	1.69 ± 0.38, 2.67 ± 0.16, 0.013 ± 0.057	6.49
J0116.8 + 6913	PowerLaw, ($N_0 \times 10^{12}$, γ)	4.73, −2.75	26.87 ± 5.81, -4.81 ± 0.23	6.77
J0008.7 + 6558	LogParabola ($N_0 \times 10^{11}$, α, β)	1.45, 2.50, 0.999	19.16 ± 6.37, 3.26 ± 0.49, 5.61 ± 0.71	7.08
J0110.2 + 6806	PowerLaw, ($N_0 \times 10^{13}$, γ)	1.95, −1.99	2.066 ± 0.081, -1.862 ± 0.064	7.17
J0000.1 + 6545	PowerLaw, ($N_0 \times 10^{12}$, γ)	1.00, −2.41	1.70 ± 0.76, -4.96 ± 1.69	7.32
J2340.7 + 8016	PowerLaw, ($N_0 \times 10^{13}$, γ)	5.68, −1.91	6.66 ± 0.64, -3.04 ± 0.19	7.37
J0152.8 + 7517	PowerLaw, ($N_0 \times 10^{14}$, γ)	1.11, −1.77	1.04 ± 0.13, -1.50 ± 0.19	7.48
J0135.0 + 6927	PowerLaw, ($N_0 \times 10^{13}$, γ)	9.57, −2.55	Removed ($TS < 5$)	7.86
J0153.4 + 7114	PowerLaw, ($N_0 \times 10^{15}$, γ)	2.31, −1.56	121.80 ± 36.24, -1.96 ± 0.13	8.28
J0204.0 + 7234	PowerLaw, ($N_0 \times 10^{13}$, γ)	3.95, −2.22	0.026 ± 0.60, -0.045 ± 0.39	8.56
J2355.5 + 8154	PowerLaw, ($N_0 \times 10^{11}$, γ)	1.0 −2.86	3.95 ± 1.23, -0.63 ± 0.13	8.87
J0025.7 + 6404	PowerLaw, ($N_0 \times 10^{14}$, γ)	4.47, −2.08	Removed ($TS < 5$)	9.13
J0051.6 + 6445	PowerLaw, ($N_0 \times 10^{13}$, γ)	2.56, −2.28	4.72 ± 121.35, -4.61 ± 32.16	9.17
J0217.5 + 7349	PowerLaw, ($N_0 \times 10^{11}$, γ)	6.13, −2.90	5.58 ± 138.71, -9.03 ± 1.73	9.21
J0001.0 + 6314	PowerLaw, ($N_0 \times 10^{12}$, γ)	8.62, −2.73	1100 ± 97, -0.63 ± 0.05	9.82
Galactic	Diffuse, (prefactor)	...	0.9842 ± 0.0018	...
Isotropic	Diffuse, (normalisation)	...	0.933 ± 0.024	...

[1] A. W. Strong, T. A. Porter, S. W. Digel, G. Johannesson, P. Martin, I. V. Moskalenko, and E. J. Murphy, Astrophys. J. **722**, L58 (2010).
[2] P. Blasi, Astron. Astrophys. Rev. **21**, 70 (2013).
[3] E. Amato, Int. J. Mod. Phys. D **23**, 1430013 (2014).
[4] M. Tavani *et al.* (AGILE Collaboration), Astrophys. J. **710**, L151 (2010).
[5] M. Ackermann *et al.* (Fermi-LAT Collaboration), Science **339**, 807 (2013).
[6] M. Cardillo, M. Tavani, A. Giuliani, S. Yoshiike, H. Sano, T. Fukuda, Y. Fukui, G. Castelletti, and G. Dubner, Astron. Astrophys. **565**, A74 (2014).
[7] A. Neronov, D. V. Semikoz, and A. M. Taylor, Phys. Rev. Lett. **108**, 051105 (2012).
[8] O. Adriani *et al.* (PAMELA Collaboration), Science **332**, 69 (2011).
[9] M. Ackermann *et al.*, Science **334**, 1103 (2011).
[10] A. M. Bykov and I. N. Toptygin, Astron. Lett. **27**, 625 (2001).
[11] Y. Butt, Nature (London) **460**, 701 (2009).
[12] M. E. Wiedebeck *et al.*, Astrophys. J. **523**, L61 (1999).
[13] J. E. Gunn and J. P. Ostriker, Phys. Rev. Lett. **22**, 728 (1969).
[14] K. Fang, K. Kotera, and A. V. Olinto, Astrophys. J. **750**, 118 (2012).
[15] M. Lemoine, K. Kotera, and J. Ptri, J. Cosmol. Astropart. Phys. 07 (2015) 016.
[16] E. Amato, D. Guetta, and P. Blasi, Astron. Astrophys. **402**, 827 (2003).
[17] J. P. Ostriker and J. E. Gunn, Astrophys. J. **157**, 1395 (1969).
[18] A. Neronov and D. V. Semikoz, Phys. Rev. D **85**, 083008 (2012).
[19] D. Hooper, P. Blasi, and P. D. Serpico, J. Cosmol. Astropart. Phys. 01 (2009) 025.
[20] W. Bednarek and M. Bartosik, Astron. Astrophys. **405**, 689 (2003).
[21] E. Amato, Int. J. Mod. Phys. Conf. Ser. **28**, 1460160 (2014).
[22] M. Hoshino, J. Arons, Y. A. Gallant, and A. B. Langdon, Astrophys. J. **390**, 454 (1992).
[23] Y. A. Gallant and J. Arons, Astrophys. J. **435**, 230 (1994).
[24] F. A. Aharonian, A. M. Atoyan, and H. J. Volk, Astron. Astrophys. **294**, L41 (1995).
[25] M. G. Aartsen *et al.* (IceCube Collaboration), Phys. Rev. Lett. **111**, 021103 (2013).
[26] A. Neronov, D. V. Semikoz, and C. Tchernin, Phys. Rev. D **89**, 103002 (2014).
[27] C. Tchernin, J. A. Aguilar, A. Neronov, and T. Montaruli, Astron. Astrophys. **560**, A67 (2013).
[28] R. Diehl *et al.*, Nature (London) **439**, 45 (2006).
[29] C. D. Ott, A. Burrows, T. A. Thompson, E. Livne, and R. Walder, Astrophys. J. Suppl. Ser. **164**, 130 (2006).
[30] N. Vranesevic *et al.*, Astrophys. J. **617**, L139 (2004).
[31] E. F. Keane and M. Kramer, Mon. Not. R. Astron. Soc. **391**, 2009 (2008).
[32] P. Blasi and E. Amato, J. Cosmol. Astropart. Phys. 01 (2012) 010.
[33] F. A. Aharonian and A. M. Atoyan, Astron. Astrophys. **362**, 937 (2000).
[34] S. R. Kelner, F. A. Aharonian, and V. V. Bugayov, Phys. Rev. D **74**, 034018 (2006); **79**, 039901(E) (2009).
[35] http://pdg.lbl.gov/2012/hadronic-xsections/.
[36] V. I. Korchagin, T. M. Girard, T. V. Borkova, D. I. Dinescu, and W. F. van Altena, Astron. J. **126**, 2896 (2003).
[37] A. W. Strong, I. V. Moskalenko, and O. Reimer, Astrophys. J. **613**, 962 (2004).
[38] G. Taylor, Proc. R. Soc. A **201**, 159 (1950).
[39] L. I. Sedov, *Similarity and Dimensional Methods in Mechanics* (Academic Press, New York, 1959).
[40] L. O. Drury, Mon. Not. R. Astron. Soc. **415**, 1807 (2011).
[41] P. R. Amnuel, O. H. Guseinov, and Iu. S. Kustamov, Astrophys. Space Sci. **121**, 1 (1986).
[42] R. N. Manchester, G. B. Hobbs, A. Teoh, and M. Hobbs, Astron. J. **129**, 1993 (2005).
[43] ATNF Pulsar Catalogue, http://www.atnf.csiro. au/people/pulsar/psrcat/.
[44] http://fermi.gsfc.nasa.gov/ssc/data/analysis/LAT_caveats.html.
[45] P. M. W. Kalberla, Astrophys. J. **588**, 805 (2003).
[46] J. Martn, D. F. Torres, and G. Pedaletti, Mon. Not. R. Astron. Soc. **459**, 3868 (2016).
[47] S. B. Popov and R. Turolla, Astrophys. Space Sci. **341**, 457 (2012).
[48] A. Noutsos, D. Schnitzeler, E. Keane, M. Kramer, and S. Johnston, Mon. Not. R. Astron. Soc. **430**, 2281 (2013).
[49] F. Acero *et al.* (Fermi-LAT Collaboration), Astrophys. J. Suppl. Ser. **218**, 23 (2015).
[50] http://fermi.gsfc.nasa.gov/ssc/data/analysis/documen-tation/Pass8_usage.html.
[51] G. Giacinti, M. Kachelriess, and D. V. Semikoz, Phys. Rev. Lett. **108**, 261101 (2012).
[52] G. Giacinti, M. Kachelriess, and D. V. Semikoz, Phys. Rev. D **88**, 023010 (2013).
[53] M. Kachelriess, A. Neronov, and D. V. Semikoz, Phys. Rev. Lett. **115**, 181103 (2015).
[54] M. S. Pshirkov, V. V. Vasiliev, and K. A. Postnov, Mon. Not. R. Astron. Soc. **459**, L76 (2016).
[55] A. A. Abdo *et al.*, Astrophys. J. **744**, 146 (2012).
[56] E. Aliu *et al.*, Astrophys. J. **764**, 38 (2013).
[57] J. P. Halpern, E. V. Gotthelf, F. Camilo, D. J. Helfand, and S. M. Ransom, Astrophys. J. **612**, 398 (2004).
[58] R. P. Mignani, A. de Luca, N. Rea, A. Shearer, S. Collins, D. F. Torres, D. Hadasch, and A. Caliandro, Mon. Not. R. Astron. Soc. **430**, 1354 (2013).
[59] M. Araya, Mon. Not. R. Astron. Soc. **444**, 860 (2014).
[60] A. Abramowski *et al.* (HESS Collaboration), Astron. Astrophys. **528**, A143 (2011).
[61] R. Kothes, B. Uyaniker, and S. Pineault, Astrophys. J. **560**, 236 (2001).
[62] V. A. Acciari *et al.* (VERITAS Collaboration), Astrophys. J. **703**, L6 (2009).
[63] C. Chang, G. G. Pavlov, and O. Kargaltsev, Astrophys. J. **744**, 81 (2012).

[64] A. Abramowski *et al.* (HESS Collaboration), Astron. Astrophys. **533**, A103 (2011).
[65] F. Aharonian *et al.* (HESS Collaboration), Astron. Astrophys. **457**, 899 (2006).
[66] A. A. Abdo *et al.* (Fermi Pulsar Timing Consortium and Fermi-LAT Collaborations), Astrophys. J. **708**, 1254 (2010).
[67] L. Bronfman, Astrophys. Space Sci. **313**, 81 (2008).
[68] B. S. Acharya *et al.*, Astropart. Phys. **43**, 3 (2013).
[69] T. DeYoung (HAWC Collaboration), Nucl. Instrum. Methods Phys. Res., Sect. A **692**, 72 (2012).
[70] http://fermi.gsfc.nasa.gov/ssc/data/analysis//scitools/source_models.html.